Approximate Bayesian Computation for an Explicit-Duration Hidden Markov Model of COVID-19 Hospital Trajectories

Gian Marco Visani* GIAN_MARCO.VISANI@TUFTS.EDU

Alexandra Hope Lee* ALEXANDRA.LEE@TUFTS.EDU

Cuong Nguyen*, M.S. CUONG.NGUYEN@TUFTS.EDU

David M. Kent[1], M.D., C.M., M.Sc. DKENT1@TUFTSMEDICALCENTER.ORG

John B. Wong[2], M.D. JWONG@TUFTSMEDICALCENTER.ORG

Joshua T. Cohen[3], Ph.D. JCOHEN@TUFTSMEDICALCENTER.ORG

Michael C. Hughes*, Ph.D. MICHAEL.HUGHES@TUFTS.EDU

* *Dept. of Computer Science, Tufts University, Medford, MA, USA*

[1] *Predictive Analytics and Comparative Effectiveness Center, Tufts Medical Center, Boston, MA*

[2] *Division of Clinical Decision Making, Tufts Medical Center, Boston, MA*

[3] *Center for the Evaluation of Value and Risk in Health, Tufts Medical Center, Boston, MA*

Abstract

We address the problem of modeling constrained hospital resources in the midst of the COVID-19 pandemic in order to inform decision-makers of future demand and assess the societal value of possible interventions. For broad applicability, we focus on the common yet challenging scenario where patient-level data for a region of interest are *not* available. Instead, given daily admissions counts, we model aggregated counts of observed resource use, such as the number of patients in the general ward, in the intensive care unit, or on a ventilator. In order to explain how individual patient trajectories produce these counts, we propose an aggregate count explicit-duration hidden Markov model, nicknamed the ACED-HMM, with an interpretable, compact parameterization. We develop an Approximate Bayesian Computation approach[1] that draws samples from the posterior distribution over the model's transition and duration parameters given aggregate counts from a specific location, thus adapting the model to a region or individual hospital site of interest. Samples from this posterior can then be used to produce future forecasts of any counts of interest. Using data from the United States and the United Kingdom, we show our mechanistic approach provides competitive probabilistic forecasts for the future even as the dynamics of the pandemic shift. Furthermore, we show how our model provides insight about recovery probabilities or length of stay distributions, and we suggest its potential to answer challenging what-if questions about the societal value of possible interventions.

1. Introduction

The ongoing COVID-19 pandemic has imposed immense costs to human health, quality of life, and the economy. There remains a pressing need for forecasting models that can reliably predict demand for scarce hospital resources, such as general-ward beds, ICU beds, ventilators, and clinical staff. It is especially important that models are likely to extrapolate to the future rather than simply repeat the past, as the pandemic evolves through new

1. Code: https://www.github.com/tufts-ml/aced-hmm-hospitalized-patient-trajectory-model

waves, new treatments, new disease variants, and the introduction of vaccines. This need naturally favors *mechanistic* models that try to capture how patients actually move through the hospital, rather than purely predictive models. Mechanistic forecasts with well-calibrated uncertainty may avoid the failures of previous COVID-19 forecasting (Ioannidis et al., 2020).

In addition to their obvious utility to hospital administrators, improved forecasting for hospital resources can also be used to assess the *societal value* of possible interventions. Throughout this pandemic, many interventions have been considered to improve outcomes for infected and hospitalized individuals, such as screening strategies, pharmaceuticals (Beigel et al., 2020; Chen et al., 2021), physical treatments (Koeckerling et al., 2020), and more (Zhang et al., 2020; Ahamad et al., 2021). However, estimating the societal value of interventions remains challenging, as they can impact many different stages of care.

Our motivating problem is to assess which interventions might avoid short-term future demand exceeding hospital capacity, as aggressive shut-downs harm other aspects of health, reduce quality of life, and restrict economic activity (Neumann et al., 2020). Policy makers, pharmaceutical companies, and funding agencies can use forecasting models to identify interventions to prioritize; such models can also inform health technology assessment and hence questions of reimbursement. But a forecast can shed light on these issues only if the model supports *"what-if"* queries about how an intervention would change patient trajectories and if the model can be *adapted* to the hospital dynamics in the region of interest.

In this work, we develop and evaluate a *mechanistic* probabilistic model of a COVID-19 patient's trajectory through stages of care in the hospital. This model can be used to make data-driven forecasts of the future daily census counts at different stages of care. That is, we can model the total count of patients in general ward, in the intensive care unit (ICU), or in the ICU on a ventilator. Importantly, the parameters driving this forecast are *interpretable* in the sense that they directly correspond to underlying mechanisms, such as transitions between stages of care and dwell-time distributions. Further, we show how our model supports asking what-if queries, such as "what if the average stay on the ventilator decreased by 2 days?", and how it quantitatively answers such questions via downstream forecasts of daily demand for hospital beds or ventilators. These forecasts could be used at a regional or hospital level to assess if utilization will exceed crucial thresholds.

Desiderata. A key design goal for our model is that it must be *portable* to health systems across the globe, so that it could accurately assess the value of an intervention in a given region or country. Healthcare system heterogeneity means that in different regions of interest, diverse data may be available due to logistical obstacles and legal concerns. To achieve portability, we assume *no* patient-level data are available (not even individualized length of stay information). Instead, our models rely only on aggregated daily count data.

A second goal is to explicitly capture uncertainty given limited data by learning a *posterior distribution* over parameters rather than a point estimate. We take a Bayesian approach by expressing our prior beliefs, updating those beliefs given some observed data, and then making the best possible predictions and decisions given remaining uncertainty (Gelman et al., 2013). Usually, fitting a posterior requires either optimization methods based on variational inference (VI) (Wainwright and Jordan, 2008), or sampling methods based on Markov chain Monte Carlo (MCMC) (Andrieu et al., 2003). However, for our model and many like it, VI and MCMC have high derivation and implementation costs even for statis-

tical learning experts, requiring months of researcher effort. These requirements make VI and MCMC difficult to use for those who need our models the most (data scientists situated inside healthcare organizations). Thus, to learn posterior distributions in ways that are accessible and extensible, we turn to simulation methods based on Approximate Bayesian Computation (ABC) (Marjoram et al., 2003; Marin et al., 2012; Cranmer et al., 2020). ABC is easy to implement given a simulation that samples from the model. Furthermore, ABC allows us to design a flexible distance function to assess fit, which we tailor to our application in ways that would be difficult with an explicit likelihood in VI and MCMC.

Contributions. This study makes three key contributions.

- First, we develop a new model capable of forecasting the daily counts of patients at various stages of care (general ward, intensive care unit (ICU), on ventilation in the ICU, death) when given the daily admissions counts. The model parameters are fully specified by fewer than 20 numbers, each one interpretable by practicing clinicians because they correspond directly to how patients move through typical hospitals.

- Second, we develop routines for fitting posterior distributions over the model's parameters given only aggregated daily count data from a region of interest. Building on Approximate Bayesian Computation (ABC) extensions of Metropolis-Hastings MCMC (Marjoram et al., 2003), we show how well-chosen distance metrics prioritizing later stages of care and recent counts, plus carefully designed annealing schedules for thresholds, enable accurate fits and forecasts for data from a target region. We further show how to scale this training to data representing *tens of thousands* of hospital stays. Because our ABC approach is simpler to implement than other possibilities, other researchers can adopt our work without advanced expertise in Bayesian learning.

- Third, we *validate* our model and posterior estimation procedures on several real-world examples from both the United States and the United Kingdom. We show that the model can provide competitive forecasts of daily counts for both a single hospital and for an entire geographic region, even when the "training" period shows rising numbers but the "testing" period exhibits falling counts due to underlying shifts in policy and population behavior. Beyond accuracy, we show that our approach can deliver *insight* into the parameters, can *scale up* to a simulation of patient pathways for all admissions in the state of California, and can be interrogated with *"what-if" scenarios* to understand the likely quantitative impact of possible interventions.

Generalizable Insights about Machine Learning in the Context of Healthcare

Many healthcare modeling problems are beset by two challenges. First, it is difficult to acquire large volumes of patient-level data (due to privacy concerns or logistical obstacles). However, relevant *aggregated* data with no patient-specific information are often publicly available. Second, it is usually easy to specify a mechanistic probabilistic model that can *simulate* individual patient trajectories and produce aggregated counts, but difficult to *learn* the posterior distribution over model parameters. Our work can be seen as a case study of lessons learned in how to apply an under-utilized methodology – Approximate Bayesian Computation (ABC) – to address both concerns in a healthcare context.

2. Related Work

Projecting the spread of COVID-19 and its impact on hospital utilization has been widely pursued. We briefly survey several threads of related work: regional modeling, local modeling (at either the hospital-level or patient-level), combinations of regional and local models, and efforts to assess societal value.

Regional modeling. Many studies have forecasted hospital utilization within a large geographic region (Murray et al., 2020; Jewell et al., 2020; Reiner et al., 2021). Some regional models use Susceptible-Infected-Recovered (SIR) models to predict regional case rates (Zou et al., 2020; Li et al., 2020), which can then inform bed usage and ventilator usage. Others (Murray et al., 2020) focus on predicting mortality rates given observed deaths, then use an internal simulation to estimate hospital utilization given fatalities.

A common limitation of regional models is their simplified and inflexible characterizations of the care pathways within hospitals. For example, CHIME[2] (Weissman et al., 2020) allows users to specify the proportions of patients requiring ICU care and mechanical ventilation, as well as the average length of stay in the hospital and in the ICU. But the model does not accommodate *distributions* for the "dwell times" at each level of care; nor does it allow for different durations among patients who recover and who deteriorate. The Imperial College model (Flaxman et al., 2020) connects deaths to key epidemiological parameters, but does not capture hospital resources. The published forecasts of the popular "IHME model" (Reiner et al., 2021), maintained by the Institute for Health Metrics and Evaluation (IHME) at the University of Washington, rely on rigid assumptions about how patients progress through the hospital (IHME COVID-19 Forecasting Team, 2020, Suppl. Sec. 8). For example, length-of-stay is not probabilistic but fixed for each class of patients (details in App. F). Users of these forecasts cannot easily modify these internal parameters or *learn* them for a location of interest; instead, the IHME itself must release updates. While the IHME model has at times performed well at its target task of accurate forecasting of mortality (Friedman et al., 2020), arguably it has been outperformed by other efforts (Gu, 2020).

Hospital-level modeling. At the hospital level, Lee et al. (2021) develop a non-mechanistic prediction model for univariate counts of COVID-19 patients at a specific hospital site based on auto-regressive statistical models. While this work is portable, we expect our mechanistic model to generalize better (as confirmed in later experiments).

Epstein and Dexter (2020) developed a mechanistic model for making hospital-specific short-term predictions of daily census counts. Given access to previous length-of-stay (LOS) information at that hospital from previous patients, they can learn distributions and forecast the length-of-stay of current patients at various stages of severity. The LOS data requirement limits portability compared to our approach.

Patient-level modeling. At the patient level, Roimi et al. (2021) developed a model to forecast an individual's hospital trajectory using personal covariates such as age and sex from thousands of patients. They built a multi-state survival model that accounts for how the patient moves day-by-day between clinical states (critical, severe, or moderate) to make local predictions for hospital resource demand in Israel. Importantly, their model accounts

2. https://penn-chime.phl.io

for many important characteristics, such as right censoring and time-dependent covariates. Our proposed model is simpler, and of course does not depend on any detailed patient-level data. Unlike our approach, it would be difficult to transfer Roimi et al. (2021)'s model across sites or regions because acquiring the necessary data is challenging.

Multi-level modeling. Recent efforts by Qian et al. (2020) present an integrated probabilistic modeling approach for COVID-19 modeling at the national, regional, hospital and individual levels, targeted at the United Kingdom. Their system, called COVID-19 Capacity Planning and Analysis System (CPAS), makes detailed hospital stay forecasts for current patients via models that utilize patient-level covariates (e.g. age, sex, comorbidities). They can further simulate the durations of future patients by sampling from an agent-based simulation, using a regional-level trend forecaster to predict admission volumes. While admirable, this kind of modeling would only be possible in a nationalized health system with access to patient-level data. For many regions of interest we simply cannot access such data.

Efforts to Assess Societal Value. A limited number of health technology assessments of COVID-19 interventions include hospital utilization projections. We have identified three. Congly et al. (2020) evaluated the administration of either remdesivir or dexamethasone to various groups of patients hospitalized to treat their COVID 19 infections. Assumptions for the model came from the literature. Gandjour (2021) assessed the addition of ICU capacity in German hospitals, using assumptions derived from information released by the German Ministry of Health. Finally, Jo et al. (2020) examined use of remdesivir and dexamethasone in South Africa. The assessment relied on clinical trial results to project therapeutic impact on length of stay and clinical outcomes. But the analysis did not explicitly describe its modeling of patient progression in the hospital setting. We emphasize that none of these analyses performed any kind of *learning or calibration* of their models to ensure consistency with observed data from the regions or sites of interest. Thus, our study advances the state-of-the-art for assessing societal value by applying modern Approximate Bayesian Computation methods to ensure that models accurately explain data from the target site.

3. Model

We now describe our proposed probabilistic model for an individual COVID patient's trajectory through the hospital. We call our model the Aggregate Counts Explicit Duration Hidden Markov Model, or "ACED-HMM" for short. While we specialize to modeling hospitalized patients with confirmed cases of COVID-19 here, the model could conceptually be used for any disease with appropriate changes to the stages of care considered as well as modified assumptions about transitions and durations.

Our proposed model represents the patient's current health state and stage of care in the hospital over a period of T days, indexed by $t \in \{1, 2, \ldots T\}$. There are 5 possible *stages*, each indicated by a unique symbol. We assume each individual patient occupies exactly one stage on each day. Fig. 1 diagrams the possible pathways and associated probabilities through these stages. There are 3 *intermediate* stages: stage **G** indicates the patient is the general ward, stage **I** indicates the patient is in the intensive care unit (but not yet on mechanical ventilation), and stage **V** indicates the patient is actively receiving mechanical

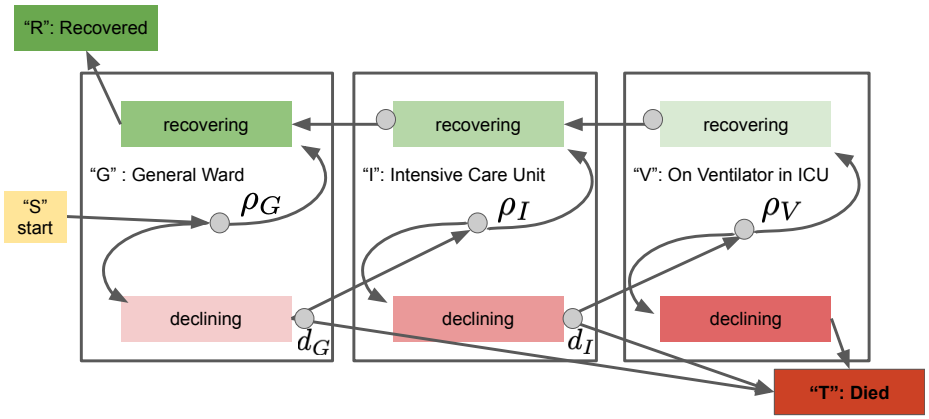

Figure 1: Diagram of the proposed Markovian model for a COVID-19 patient's trajectory through the hospital. Rectangles indicate possible states, defined by the patient's current stage of care s (general ward **G**, off ventilator in ICU **I**, on ventilator in ICU **V**) as well as health trajectory h (recovering or declining). Small circles indicate stochastic binary choices, with one path marked by transition probability. Recovery transition parameters ρ_k give the chance of switching to a recovery path, while early death probabilities d_k mark the chance of dying early. Based on clinical advice, the early death probabilities d_G and d_I are modeled as very small under the prior. Each state has an explicit duration distribution (not shown).

ventilation in intensive care. There are additionally 2 possible *absorbing* or *terminal* stages: "terminal death" **T** or "fully recovered" **R**.

For each patient, indexed by n, our model generates a sequence of care segments indexed by ℓ, with total length L_n (not all patients will experience the same number of segments). Each segment is defined by a "stage" category indicator $s_{n\ell} \in \{\mathbf{G}, \mathbf{I}, \mathbf{V}, \mathbf{R}, \mathbf{T}\}$, a "health" binary indicator $h_{n\ell} \in \{0, 1\}$ corresponding to a "declining" or "recovering" trajectory within that segment, and a "duration" integer $\Delta_{n\ell} \in \{1, 2, \dots D\}$ representing the number of *days* spent in that care segment. Our model generates patient n's sequence of stage indicators $s_{n,1:L_n}$, health indicators $h_{n,1:L_n}$, and durations $\Delta_{n,1:L_n}$ via the random process defined below. We drop the patient index n below when it is clear we are talking about one patient to keep notation simple.

We stress that our model assumes that for each patient, we are given an integer $a_n \in \{1, 2, \dots, T\}$ indicating the day the patient was *admitted* to the hospital. Throughout this paper, we assume all patients begin in the general ward on their first day. However, in principle it is easy to capture incoming patients that directly begin in the ICU stage **I** or on the ventilator **V**, which might realistically happen for a transfer patient referred to a large facility with more specialty care or available ICU beds.

3.1. The ACED-HMM Generative Model

Generating stage indicators. We always start in the general ward, and generate the new *stage* indicator $s_\ell \in \{\mathbf{G}, \mathbf{I}, \mathbf{V}, \mathbf{R}, \mathbf{T}\}$ for each subsequent segment $\ell \in 2, 3, \dots$ given the previous health indicator $h_{\ell-1}$ via:

$$s_1 \leftarrow \mathbf{G}, \quad s_\ell \leftarrow \begin{cases} \mathbf{T} & \text{w. prob. } d_{s_{\ell-1}} \text{ if } h_{\ell-1} = 0 \\ \text{next\_stage}(s_{\ell-1}, h_{\ell-1}) & \text{otherwise} \end{cases} \tag{1}$$

where parameters $d_{\mathbf{G}}$ and $d_{\mathbf{V}}$ define the chance of early death, and the deterministic `next_stage` procedure always advances in order $[\mathbf{G}, \mathbf{I}, \mathbf{V}, \mathbf{T}]$ if health is declining ($h_{\ell-1} = 0$), and to advance in order $[\mathbf{V}, \mathbf{I}, \mathbf{G}, \mathbf{R}]$ if health is recovering ($h_{\ell-1} = 1$). See Fig. 1 for visual illustration of these stage pathways. Once we reach either absorbing stage ($\mathbf{R}$ or $\mathbf{T}$), we halt all further generation (this event defines the sequence length L_n).

Generating health indicators. We generate the health indicator for segment ℓ, $h_\ell \in \{0, 1\}$, given the previous health indicator $h_{\ell-1}$ and the new stage s_ℓ. After each declining segment ($h = 0$), we switch to recovery with a stage-specific recovery probability $\rho_k \in [0, 1]$, but otherwise keep declining. Once on a path to recovery (indicated by $h = 1$), we assume the patient stays there and continues to recover:

$$h_\ell \leftarrow \begin{cases} 1 \text{ if } h_{\ell-1} = 1 \\ u \text{ if } h_{\ell-1} = 0, \quad u \sim \text{Bern}(\rho_{s_\ell}), \end{cases} \qquad \ell \in \{1, 2, \ldots\}. \tag{2}$$

The parameters here are the recovery probabilities ρ_k for each intermediate stage $k \in \mathcal{K}$ where $\mathcal{K} \in \{\mathbf{G}, \mathbf{I}, \mathbf{V}\}$.

Generating durations. We generate the duration (in days) Δ_ℓ for segment ℓ as:

$$\Delta_\ell | s_\ell, h_\ell \sim \text{Cat}(\pi_1^{s_\ell, h_\ell}, \ldots \pi_D^{s_\ell, h_\ell}). \tag{3}$$

where probability vector $\pi^{k,h}$ defines a categorical probability mass function over the first D integers $\{1, 2, \ldots D\}$. This vector defines the distribution over possible durations spent at stage $k \in \mathcal{K}$ while in health state $h \in \{0, 1\}$. Notably, this model flexibly allows recovering ($h = 1$) and declining ($h = 0$) patients to have different duration distributions at each stage.

Here, for tractability we must define the maximum number of days D allowed in each segment. To balance reasonable computation times while matching some of the long stays observed for this disease, we set $D = 22$. Designation of this value as our maximum duration at any segment of hospital care reflects statistics from the U.S. CDC as of September 2020 (CDC, 2020, Table 2). The CDC data indicates that for patients admitted to the ICU, the 75th percentile estimated for *total hospital length of stay* (which corresponds to many segments of our model) ranges from 20 days to 25 days across age groups. For patients not admitted to the ICU, stays are typically much shorter. Thus, truncation of stage-specific durations at 22 days affects few real-world patients and should still yield accurate forecasts.

Tractable parameterization of durations. As written above, we need to learn a separate $D-$dimensional probability vector $\pi^{k,h}$ for each state (indexed by stage k and health h). We decide to explore a simpler formulation with only two scalar parameters per state: mode location $\lambda^{k,h} > 0$ and temperature $\nu^{k,h} > 0$:

$$[\pi_1^{k,h}, \ \ldots \ , \pi_D^{k,h}] \leftarrow \text{softmax}\left(\frac{\log \text{PoiPMF}(1|\lambda^{k,h})}{\nu^{k,h}}, \ldots, \frac{\log \text{PoiPMF}(D|\lambda^{k,h})}{\nu^{k,h}} \right). \tag{4}$$

where PoiPMF denotes the probability mass function of the Poisson distribution. See Figure 2 to see how the distribution π over D days depends on these two parameters. Intuitively, $\lambda^{k,h}$ controls the location of the mode. Large temperatures $\nu^{k,h} \gg 0$ makes the distribution $\pi^{k,h}$ more uniform, while as $\nu^{k,h} \to 0$ the distribution becomes peaked at the mode. This flexible parameterization encodes two valuable inductive biases: similar stay-lengths have similar probabilities, and the overall distribution is either unimodal or flat. This 2-parameter

formulation has been previously used for supervised modeling of ordinal outcomes (Beckham and Pal, 2017), but to our knowledge is new for durations in a semi-Markov model.

Joint Probability Distribution. Each patient's entire observable experience can be captured by sequences of stage indicators, health indicators, and durations $s_{1:L_n}, h_{1:L_n}, \Delta_{1:L_n}$, with joint probability:

$$p(s_{1:L_n}, h_{1:L_n}, \Delta_{1:L_n}) = p_\tau(s_1, h_1) \prod_{\ell=2}^{L_n} p_\tau(s_\ell, h_\ell | s_{\ell-1}, h_{\ell-1}) \cdot \prod_{\ell=1}^{L_n} p_\xi(\Delta_\ell | s_\ell, h_\ell) \quad (5)$$

Here we've gathered all transition probabilities into τ, such that $\tau = \{d, \rho\}$ and all duration parameters are denoted $\xi = \{\lambda, \nu\}$ for simplicity. Notably, this model structure can be mapped to the semi-Markov model known as an explicit-duration (hidden) Markov model (Ferguson, 1980; Mitchell and Jamieson, 1993; Yu, 2010), by mapping the health and stage indicator variable sequences $h_{1:L_n}$, $s_{1:L_n}$ to a discrete state sequence $z_{1:L_n}$ with 9 possible states: the start state $\mathbf{S}$, the two absorbing states $\mathbf{T}, \mathbf{R}$, and 6 intermediate states $\mathbf{G}0, \mathbf{G}1, \mathbf{I}0, \mathbf{I}1, \mathbf{V}0, \mathbf{V}1$ where the 0 (1) suffix in the state name represents the declining (recovering) variant of each stage, respectively. The transition probability parameters for this HMM are specified in Supplementary Table C.1. Throughout the rest of the paper, we use the compact notation $\mathbf{z}_n = z_{1:L_n}$ below to capture the state sequence for patient n, which can be easily mapped back to the stage sequence and health sequence.

3.2. Prior beliefs about transition and duration parameters

Priors on transition parameters. We can use published statistics to inform our prior beliefs about transition probability parameters $\tau = \{\rho, d\}$. Published probability statistics from the U.S. Centers for Disease Control (CDC) (see Table 2 of CDC (2020)) indicate the fraction of hospitalized COVID-19 patients who are admitted to ICU, placed on the ventilator, and eventually die, for each of three age groups (18-49, 50-64, and 65+). We translate these into Beta priors for each ρ_k that try to match the mean of these statistics while covering the overall possible range across age groups. See Appendix C.2 for details.

We next set the early death probabilities. Based on conversations with clinical experts, we expect the chance of early death in the general ward is very low ($\mathbb{E}[d_{\mathbf{G}}] \approx 1\%$) and the chance of early death in the ICU is only slightly larger ($\mathbb{E}[d_{\mathbf{I}}] \approx 2\%$). We again set Beta priors to match these means and produce little uncertainty around them (such that the 95th percentile is below 0.05) to reflect our confidence that early death is possible but rare.

Priors on duration parameters. To determine priors over the durations spent in each state (indexed by s, h), we draw relevant parameters independently from a common prior:

$$\lambda^{s,h} \sim \mathcal{N}(\mu^{s,h}, (\sigma^{s,h})^2, lower = 0, higher = D), \quad \log_{10} \nu^{s,h} \sim \mathcal{N}(0.5, 0.5^2). \quad (6)$$

Visuals of our prior's imposed distribution on durations in each state can be seen in Fig. 5.

Our truncated normal prior for the mode location $\lambda^{s,h}$ of each state reflects that these quantities are difficult to know without reliable data about previous patient experience in the region or site of interest. We select a mean of $\mu^{s,h} = 8$ days with a *high* standard deviation $\sigma^{s,h} = 3$, such that our Normal prior's range of likely values ($\mu^{s,h} \pm 3\sigma^{s,h}$, covering over 99% of probability mass) could plausibly set the duration mode from 1 to 17 days.

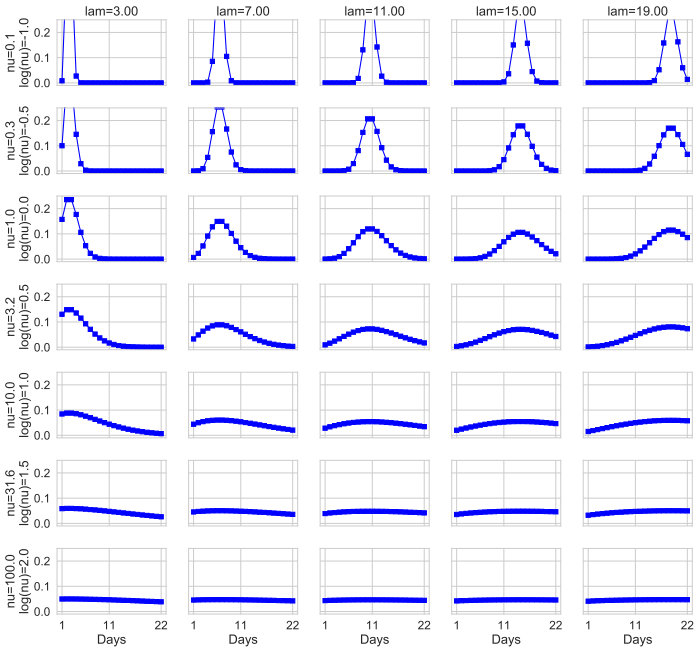

Figure 2: Visualization of possible duration distributions under our proposed tractable 2-parameter family. Parameter $\lambda > 0$ (x-axis) controls the location of the mode, while the temperature parameter $\nu > 0$ (y-axis) controls the entropy around this mode.

Our prior for each state's temperature $\nu^{s,h}$ assumes the *log* of this value will be normally distributed. By using a prior for $\log_{10} \nu^{s,h}$ with mean 0.5 and standard deviation 0.5, we allow plausible temperatures to span both high and low entropy distributions.

4. Learning

In order to train our model so its parameters reasonably explain hospital trajectories in a specific region or site of interest, we assume we have access to some observed daily counts $\mathbf{y}_{1:T} = \{y^k_{1:T}\}_{k \in \mathcal{K}}$ during the training time period of interest. Here the set of observed stages $\mathcal{K}$ could include any of the intermediate or terminal stages; typically $\mathcal{K} = \{\mathbf{G}, \mathbf{I}, \mathbf{V}, \mathbf{T}\}$. We also assume knowledge of the admission counts $a_{1:T}$ for the training period, which represent a total of N patients who enter the hospital system, with $N = \sum_{t=1}^{T} a_t$.

Given observed counts $\mathbf{y}_{1:T}, a_{1:T}$, we wish to be able to draw samples from the posterior $p(\tau, \xi, \mathbf{z}_{1:N}, \mathbf{\Delta}_{1:N} | \mathbf{y}_{1:T}, a_{1:T})$. Samples from this distribution allow us to properly understand the range of possible values for the model's transition parameters τ and duration parameters $\xi = \{\lambda, \nu\}$. Samples of parameters can further allow us to produce *forecasts*, as we can draw samples of counts $\mathbf{y}_{T+1:T+F}$ for a "testing" period of F days – $T+1, \ldots T+F$ – by taking some assumed admissions $a_{T+1:T+F}$ for this period drawing samples forward.

For our model, it is easy to *simulate* patient care sequences and to produce aggregate counts from these sequences (simply counting the total number of patients simulated in each stage at each day). However, it is cumbersome to define an explicit probability mass function for both the individual patient care sequences $\mathbf{z}_n, \mathbf{\Delta}_n$ and the observed aggregate counts $\mathbf{y}_{1:T}$. This would only become more difficult if we explore more complex versions

of our model down the road (e.g. add age-dependent transition or duration probabilities). We would like to be able to simply define a *simulation* that produces samples of aggregate counts, and then be able to (approximately) fit its distribution to observed count data.

4.1. Approximate Bayesian Computation

To achieve this desired goal, we turn to Approximate Bayesian Computation (ABC) (Marjoram et al., 2003; Marin et al., 2012; Cranmer et al., 2020), a method for fitting models that are naturally expressed as simulations. ABC has found applications in ecology (Beaumont, 2010), population genetics (Beaumont et al., 2002), and epidemiology (Blum and Tran, 2010). ABC is useful in cases like ours, where standard Markov chain Monte Carlo methods would require an explicit ability to compute the likelihood of observed counts arising from our individual simulations. ABC offers a simpler approach: we need only the ability to simulate counts and the ability to decide if simulated counts are "close enough".

Our approach is based on the ABC MCMC algorithm presented by Marjoram et al. (2003). We iteratively propose new candidate values for parameters τ, ξ, and then decide to accept or reject these based on an acceptance criterion designed to ensure the overall sequence of sampled parameters converges to the target posterior distribution. This looks superficially similar to conventional Metropolis-Hastings MCMC (Metropolis et al., 1953; Andrieu et al., 2003). However, the test for acceptance uses an evaluation of a distance function d between observed data $\mathbf{y}_{1:T}$ and our simulation's sampled counts $\tilde{\mathbf{y}}_{1:T}$. This distance threshold check replaces the evaluation of an explicit likelihood (which would require specification of a probability mass function and the ability to evaluate it efficiently).

An advantage of our ABC approach is we do not need to compute or even define an explicitly probability distribution for the likelihood $p(\mathbf{y}_{1:T}|\mathbf{z}_{1:N}, \mathbf{\Delta}_{1:N})$. This allows us to avoid a potentially detrimental *misspecified* parametric form chosen for computational convenience. Furthermore, another advantage of ABC is that we can easily customize the distance function to meet application-specific needs; specifying a full likelihood distribution that acheives the same goals might be more challenging. For example, our chosen distance below encodes an emphasis on fitting the most recent daily counts in the training period (so our forecasts will generalize to the future well) and an emphasis on later stages of the model (since those are harder to estimate well).

Distance computation. Given the set of $\mathcal{K}$ observed stages, let K denote the number of stages $K = |\mathcal{K}|$. Then y_t^k denotes the observed count at time t observed from stage k, and $\tilde{y}_t^k$ denotes the simulation's sampled count. We define the distance as a normalized weighted mean-absolute-error:

$$d(\mathbf{y}_{1:T}, \tilde{\mathbf{y}}_{1:T}) = \frac{1}{K \cdot T} \sum_{t=1}^{T} \sum_{k=1}^{K} w_{tk} \frac{|y_t^k - \tilde{y}_t^k|}{\max(y_t^k, \tilde{y}_t^k)} \tag{7}$$

where w_{tk} is a scalar weight that determines the relative "importance" of matching the counts at time t and stage k. We define w_{tk} as a product of a time-specific weight v_t and a stage-specific weight u_k. For timestep weight v_t, we apply a recency bias: we linearly interpolate between $v_1 = 0.5$ at day 1 and $v_T = 1.5$ at day T, so that our model is better at making forecasts after day T (and the average timestep weight is 1). We use stage-specific weights u_k because preliminary experiments suggested that counts for the *later* stages of

the model are harder to fit (since all N patients enter the general ward, but only a smaller fraction will reach the ICU and the ventilator). Thus, we set u_k values so later stages are worth more. Our recency emphasis via weights v_t and later-stage emphasis via weights u_k are both important for good forecasting results in our application, and would be difficult to encode in an explicit likelihood as in traditional MCMC. See Appendix D for details and further discussion of our chosen distance.

Proposal distributions q. Our ABC algorithm requires a procedure to draw a new plausible parameter value given a current value. For each type of parameter (transition probabilities, duration modes, duration temperatures), we define a simple "random walk" proposal distribution q with the mean at the "old" value and a variance that encourages modest exploration. See Appendix D for parameter-specific details.

ABC algorithm. Initial values of the transition parameters τ and duration parameters ξ are samples from our chosen priors $p(\tau)$ and $p(\xi)$ defined above. Then, until convergence, the algorithm visits each individual parameter in turn (e.g. either a specific transition probability parameter ρ_k or d_k within τ, or a state-specific duration mode $\lambda^{s,h}$ or temperature $\nu^{s,h}$ within ξ). At each visit, a new candidate value is proposed from our chosen distribution q (defined above). Then, we decide whether to "accept" or "reject" that value. For simplicity, we denote the current set of parameters as τ, ξ, and the new candidate parameters (with one entry updated) as τ^*, ξ^*.

There are two stages of acceptance. First, counts are simulated from our ACED-HMM progression model for the entire training period using the proposed parameters τ^*, ξ^*, generating $\tilde{y}_{1:T}$. Then, we compute the distance d between the samples $\tilde{\mathbf{y}}_{1:T}$ and true counts $\mathbf{y}_{1:T}$. If the distance d is below a chosen distance tolerance threshold ε, the algorithm moves on to the second stage of acceptance, otherwise the proposed parameters are rejected. Second, the proposed parameters are accepted if a random uniform draw between 0 and 1 is less than the acceptance ratio $\alpha = \frac{p(\tau^*,\xi^*)q(\tau^*,\xi^*\to\tau,\xi)}{p(\tau,\xi)q(\tau,\xi\to\tau^*,\xi^*)}$. The first stage of acceptance checks the fit to the data (replacing the likelihood used in conventional MCMC), whereas the second stage further filters the acceptance via information from the prior and from the proposal to maintain the validity of the target distribution of the Markov chain (Marjoram et al., 2003).

Scheduling the distance tolerance threshold. Because random initial parameters are unlikely to explain observed data well, we find it useful to start from a lenient value of the data-agreement threshold ε. i.e. one that accepts all proposals. We then decay ε across iterations to a value that better ensures a match to observed data. In the Supplement Sec. D, we describe two phases for our ABC algorithm: a *burn-in* phase and a *sampling* phase. In *burn-in*, we gradually decay the value of ε over many iterations to reach a good explanation of the data. Then, in *sampling* we hold ε fixed and collect parameter samples, which are treated as representative of the target posterior distribution. During burn-in, we find it helpful to periodically *increase* ε sharply and then decay gradually to escape local optima. See Fig. D.1 for a visual representation of escaping a local optima using this idea.

Ensembling. In order to obtain robust estimates of the posterior, we combine samples from multiple independent runs of our ABC algorithm into an ensemble. For any given dataset, we expect there might be several different parameter configurations that explain the training counts well (due to the flexibility of the model and possible identifiability issues

given limited counts). Ensembling allows us to capture more of these configurations than a single run of ABC might recover. By aggregating, we gain statistical strength in the forecasts as well as a deeper understanding of the uncertainty in learned parameter values.

Synthetic validation. We conducted several experiments on synthetic "toy" datasets (generated by our model) to verify that our ABC procedures can (approximately) recover plausible posterior distributions. See Appendix B.3 for a thorough description.

5. Data for Case Studies

We consider fitting our proposed model to pursue two possible applications over a range of geographic scales. First, as a primary use case we consider performing *regional* forecasts, specifically for several states in the United States. State-level modeling allows us to make forecasts that interest policy makers and public-health officials within that state. We'll also show how these forecasts might be used to assess societal value. Second, we consider performing *site-level* forecasts for specific hospitals in the United Kingdom (UK). These experiments allow us to assess potential utility to hospital administrators for planning purposes.

Below, we describe the data acquired for training and evaluating our forecasting model in both cases. Each dataset is assumed to provide census counts for the training period, denoted as days $1, 2, \dots T$, for some subset or additive combination of the stages of our model (general ward $\mathbf{G}$, off-ventilator in ICU $\mathbf{I}$, on-ventilator in ICU $\mathbf{V}$, terminal death $\mathbf{T}$). To evaluate forecasts against a "ground truth", we further require the same counts for the future period of interest, starting on day $T+1$ and ending on $T+F$.

In order to assess our proposed hospital progression model, during both training and forecasting we assume access to true daily *admissions* counts to the general ward. For a real forecast after day T, these counts will not be known. In this case, we could use hand-designed counts representing plausible future admission count scenarios provided by clinical experts. Alternatively, we could use any forecasting model to produce future admission counts (such as the model by Qian et al. (2020)). In this work, we assume admissions are all directly into the general ward. This could be easily changed if desired (e.g. to simulate the impact of transfers from an external hospital directly into the target hospital's ICU).

5.1. U.S. state hospital data for regional forecasts

We obtain hospital utilization counts for four US states: Massachusetts (MA), Utah (UT), South Dakota (SD), and California (CA). We use counts from November 11th, 2020 to January 11th, 2021 as training data, and forecast one month into the future. These chosen states were selected to represent diverse geographic regions as well as diverse hospital utilization dynamics and policy responses to the pandemic during the selected time period. For example, hospitalizations in SD peaked in late November, in MA in early January, and in UT in late January.

For all states, we use data from the COVID Tracking Project (The Atlantic Monthly Group, 2021)[3] and the U. S. Dept. of Health and Human Services (2021)[4]. See Appendix A

3. https://covidtracking.com/data
4. https://healthdata.gov/Hospital/COVID-19-Reported-Patient-Impact-and-Hospital-Capa/g62h-syeh

for details on how we collected the data. At the end of data collection, for each state we have access to a daily time series of General Ward ($\mathbf{G}$) counts, counts in the ICU off the ventilator ($\mathbf{I}$), counts on the ventilator ($\mathbf{V}$) and terminal death counts ($\mathbf{T}$). For Utah and California in particular, we have access only to aggregate ICU counts ($\mathbf{I}+\mathbf{V}$) that do not distinguish between on and off the ventilator. For all states, we found that *smoothing* the terminal counts produced more sensible data (in the raw data, some weekends and holidays report implausibly low counts for deaths that reflect imperfect reporting processes).

5.2. United Kingdom hospital data for site-level forecasts

We obtain daily occupancy counts at different care stages from two U.K. hospitals: South Tees and Oxford University, made available to the public by the UK National Health Service[5]. We use counts from November 3rd to January 3rd as training data, and forecast one month into the future (counts past February 3rd were unavailable when we ran the experiments). We selected these two hospitals because they represented large daily volumes and appeared to have higher-quality data with fewer irregularities than other alternatives. After data collection (see details in Appendix A), for each site we had access to counts of total beds used ($\mathbf{G}+\mathbf{I}+\mathbf{V}$), counts on the ventilator ($\mathbf{V}$), and daily counts of recovered patients discharged from the hospital (stage $\mathbf{R}$ of our model).

6. Results of Case Studies

Below, we describe a range of experimental results that assess our model's qualitative and quantitative performance as well as scalability, sensitivity to available data, and ability to answer what-if questions.

6.1. Forecast assessment: Can this model capture qualitative trends?

We show our method's forecasted distribution over daily counts for the entire US state of Massachusetts in Fig. 3. Importantly, we see that our ACED-HMM mechanistic model (blue lines), trained only on periods of *rising* case numbers, can reasonably forecast during the *downward* trend in hospital counts seen in MA after mid-January 2021. In contrast, a baseline non-mechanistic auto-regressive prediction model (red line, App. E), inspired by Lee et al. (2021), does not generalize well in the testing period.

We further examine a forecast for a specific hospital site in the UK ("South Tees") in Fig. 4. Here, we see how our method can accurately capture *rising* trends during the evaluation period for both overall occupied beds (the sum of several stages: $\mathbf{G}+\mathbf{I}+\mathbf{V}$) as well as for the number of ventilators in use (stage $\mathbf{V}$), despite the fact that during the training period the counts were mostly flat and had only recently begun to rise. These results indicate that our model's learned transition and duration distributions can successfully *translate* several weeks into the future in some cases. Again, we do stress that we provided our model the true admission counts for the testing period. However, accurate ventilator demand prediction depended on and hence implies accurate transition and duration modeling.

5. https://www.england.nhs.uk/statistics/statistical-work-areas/covid-19-hospital-activity/

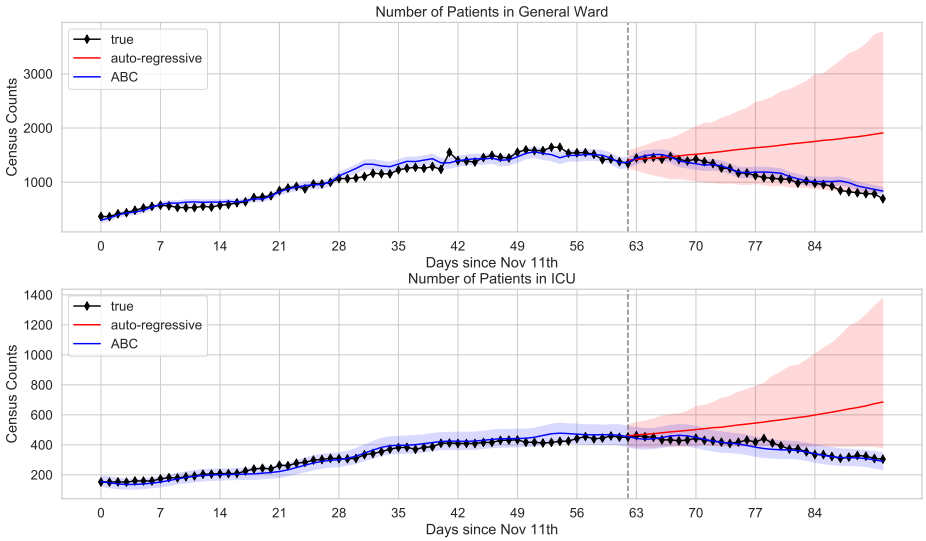

Figure 3: **Fit and forecasts on General Ward (G) and Total ICU (I + V) counts for Massachusetts.** We use our ABC procedure to estimate an approximate posterior over our progression model's parameters, using 2 months of counts (left of the vertical dashed line). We stress that our ABC method is also provided true daily admission counts for all days (0 - 92). We also include a forecast from a baseline competitor model fit to the last 28 days of the training period (a statistical autoregressive model with Poisson likelihood, See E), to highlight advantages of our mechanistic model. Shaded intervals show the 2.5th and 97.5th percentiles of 2000 posterior samples.

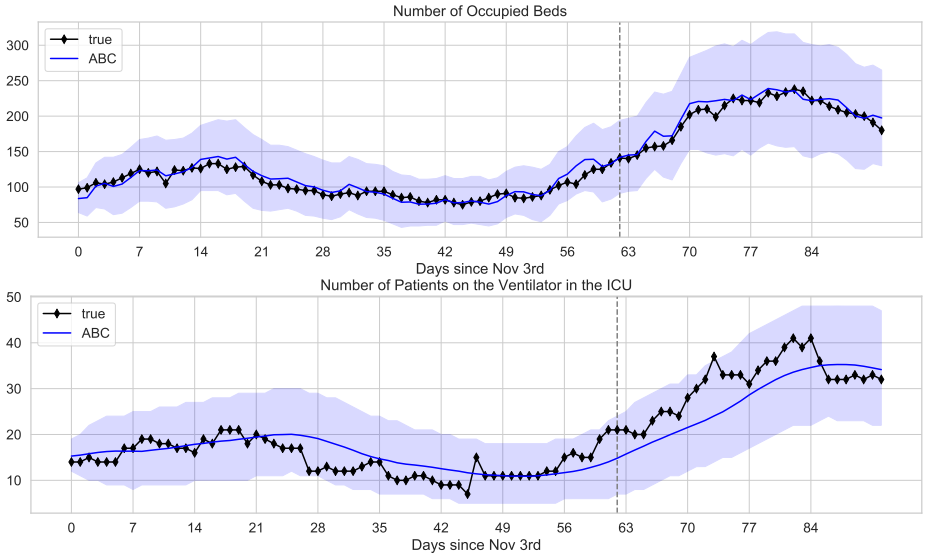

Figure 4: **Fit and forecasts on Occupied Beds and Ventilator counts for South Tees hospital in the UK.** Parameters were selected via ABC to fit 2 months of counts (November 3rd to January 3rd, left of the vertical dashed line). Shaded intervals show the 2.5th and 97.5th percentiles of 2000 posterior samples.

6.2. Quantitative assessment: How accurate are forecasts?

We quantitatively evaluate the quality of our method's forecasts for 3 US states and 2 UK hospitals. For all U.S. states, we compare to forecasts from the IHME model (Reiner et al., 2021). For one US state and one UK hospital, we also compare our method's forecasts to two baselines: a statistical autoregressive model with Poisson likelihood, and our prior over ACED-HMM's parameters. We consider two quantitative evaluation metrics, highlighting the results of each below.

First, we compute Mean Absolute Error (MAE), to assess the error between each method's mean prediction and the observed daily counts in the testing period. See MAE results for the US (Tab. B.1) and the UK (Tab. B.2) in Appendix B.1. For MA (a larger state with over 5.5 million adult residents), the key takeaway is that our ABC method achieves state-wide MAE below 65 across all stages, while other methods are considerably larger in most cases (for general ward, our MAE is 65 while others are all above 490; for ICU our MAE is 15.7 while others are above 100). While IHME achieves slightly better MAE on ventilator counts from MA than our method, it overshoots the general ward counts considerably. For the two smaller states (SD and UT, each with fewer than 3 million adult residents), our mean absolute error (MAE) across all stages remained below 21, while other methods are considerably worse (e.g. the IHME baseline exceeds 100 MAE for the ICU in UT and exceeds 71 MAE for the general ward in SD). The results illustrate that our method can produce forecasts with small deviation from the ground truth across several diverse scenarios.

Second, we assess the *coverage* of the learned posterior distribution across the 50%, 80% and 95% centered intervals of the posterior. For an ideal, well-calibrated posterior, we should observe that X% of the actual counts in the testing period fall within an interval chosen to cover X% of the distribution's mass. See results for the US (Tab. B.3) and the UK (Tab. B.4) in Appendix B.2. We find the coverage of our ACED-HMM is more plausible than baselines, though there is still room to improve as we might expect from knowing our model is an approximation of reality.

6.3. Interpretation of learned posteriors over parameters

In Fig. 5, we show the learned posterior distributions over *all* relevant model parameters after fitting on the Massachusetts data. Several insights regarding hospital dynamics in MA can be drawn. For instance, the learned probability of recovering in $\mathbf{I}$ is significantly lower than that indicated by the prior, indicating a potential deviation in hospital dynamics or in the patient age distribution in MA compared to the US as a whole. The learned posterior indicates, with high confidence, that the average length of stay in $\mathbf{I}$ (ICU *not* on the ventilator) is very low, both for recovering ($h = 1$) and especially for declining ($h = 0$) patients, indicating that a patient who is on a declining path in the ICU is very quickly moved to the ventilator. Last, patients on the ventilator seem to stay there for shorter periods of time when *declining* rather than when *recovering*. However, we note that the duration posterior for recovering on the ventilator closely matches the prior and is bimodal, indicating we may not be confident that the posterior has recovered the "ideal" parameter. This result is not surprising, as very few of all admitted patients recover from the ventilator, and thus given limited data it is the most difficult of all parameters to recover.

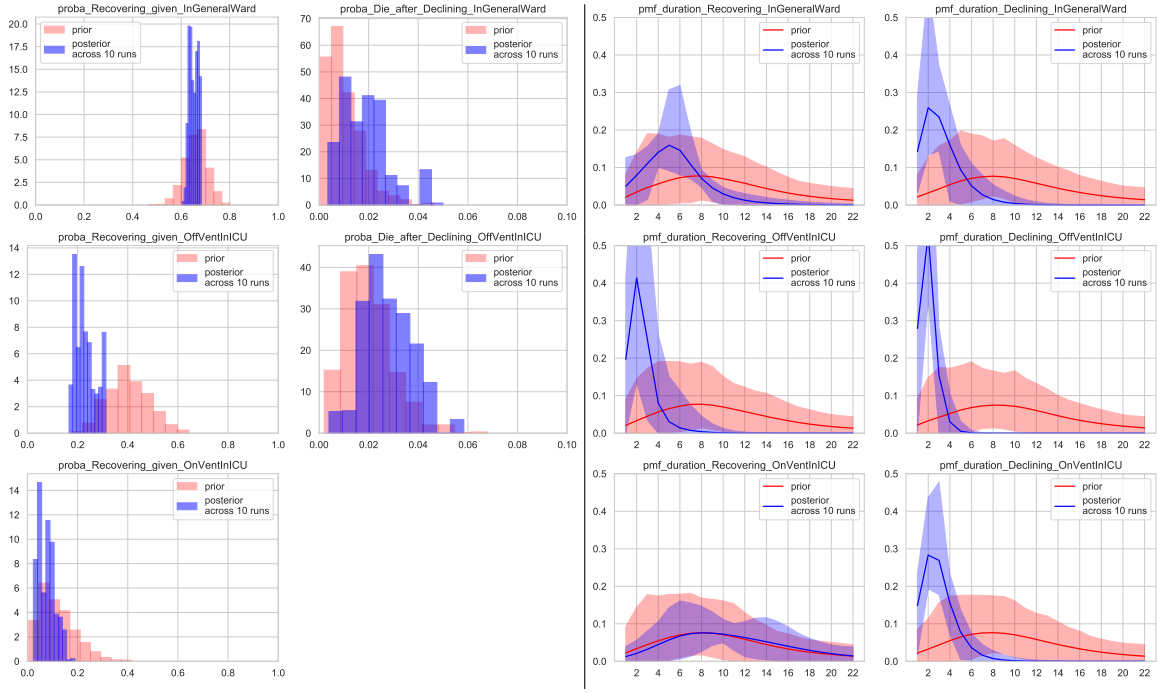

Figure 5: **Posterior distributions over parameters for Massachusetts (Nov. 11 - Jan. 11).** We show transition parameters (left) and duration parameters (right) after fitting on 2 months of counts, where each day we used available census counts for $\mathbf{G}, \mathbf{I}, \mathbf{V}$, and $\mathbf{T}$. The colored interval of duration plots shows the 2.5 - 97.5th percentile intervals of 2000 samples (10 runs, each with 200 samples). The prior is also shown for comparison.

In Fig. B.1 in the Appendix, we further visualize the learned posteriors for the South Tees hospital site in the UK. As expected, we observe much higher variance in these learned posteriors than the posteriors for the (much larger) Massachusetts dataset above. Naturally, for a single hospital site we expect to be more uncertain (less confident). However, we notice some potentially valuable differences compared to MA. Duration distributions appear to be longer, and patients appear to be more likely to recover both in the General Ward and in the ICU.

6.4. Data ablation study: How does learning from different sets of counts affect the learned posterior?

Public data sources may differ in terms of the granularity of available counts. For example, for U.S. states we can usually gather separate counts of for each of the $\mathbf{G}, \mathbf{I}$, and $\mathbf{V}$ intermediate stages as well as the terminal stage $\mathbf{T}$, while for the U.K. we only have counts of all beds ($\mathbf{G} + \mathbf{I} + \mathbf{V}$), patients on ventilation ($\mathbf{V}$), and recovered ($\mathbf{R}$). Other sites may yet offer other different subsets of $\{\mathbf{G}, \mathbf{I}, \mathbf{V}, \mathbf{T}, \mathbf{R}\}$.

To assess the model's sensitivity to data granularity, we trained the ACED-HMM on the Massachusetts data we used in our other experiments, but with a key manually imposed difference in available data: instead of fitting to the finest granularity of available counts – $\mathbf{G}$, $\mathbf{I}$, $\mathbf{V}$ and $\mathbf{T}$ separately – we instead aggregate all intermediate stages and fit the parameters

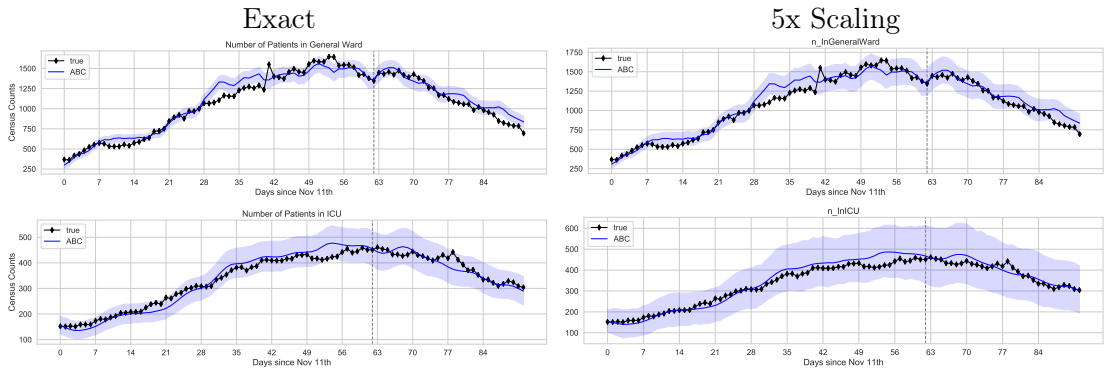

Figure 6: **Scalability assessment for MA data.** We show the predictions for our ABC method using all admissions recorded in the training period (left), as well as our proposed scaling procedure with a 5x scale factor (right). The scaling simulates only 20% of observed admissions but then scales all counts by 5. The scaling procedure allows simulations to run 5 times faster with the same qualitative trend recovery and only modest increases in uncertainty intervals.

to daily counts of all beds ($\mathbf{G}+\mathbf{I}+\mathbf{V}$) and death ($\mathbf{T}$) only. See Fig. B.2 for fits and forecasts to $\mathbf{G}$, $\mathbf{I}$, $\mathbf{V}$ and $\mathbf{G}+\mathbf{I}+\mathbf{V}$ counts, and Fig. B.3 for the learned model parameters.

We find that, while the model trained with less-granular data can fit the aggregate "all beds" counts well in both training and test periods, the model could not recover individual stage counts from the $\mathbf{G}$ and $\mathbf{I}$ stages well. In particular, the algorithm converged to parameters that undershot $\mathbf{G}$ counts and overshot $\mathbf{I}$ counts. The differing signs of these errors roughly cancel out and thus aggregate counts are predicted well. Interestingly, the model managed better predictions of $\mathbf{V}$. We believe this is due to the presence of $\mathbf{T}$ counts at training time, as these values provide a more direct signal for what the $\mathbf{V}$ counts should be.

This experiment shows that, as expected, forecasts on fine-grained counts that the model was not trained on are generally not reliable, unless some closely-related counts is provided (e.g. $\mathbf{T}$ is provided as a signal for $\mathbf{V}$ or $\mathbf{R}$ is provided as a signal for $\mathbf{G}$). Stronger, more informative priors about the intermediate stages may also improve performance when fine-grained signals are not available.

6.5. Scalability assessment: How well does this model scale?

A key design requirement of our procedure is scaling up our simulations to handle data from large regions or even entire countries. We propose a simple but effective scaling procedure for ABC algorithm: given a scaling factor $r > 1$, we simulate only a fraction $\frac{1}{r}$ of all admissions (at a fraction the computational cost). Then we multiplicatively rescale the resulting aggregate counts produced by the simulation appropriately: $r\tilde{y}_t^k$. In expectation, this should be an unbiased estimator of simulated counts from the full admitted population. In Fig. 6, we show that our proposed scaling procedure is effective. Simulating only 20% of admissions in MA and rescaling, we see a qualitatively similar recovered forecast with only modestly increased uncertainty. With exact simulation of Massachusetts already feasible, by applying 10-x or 20-x scaling we can easily forecast for any U.S. state of interest.

6.6. What-if scenario assessment: Can we assess the impact of interventions?

We now consider using our model to make data-driven decisions to assess the value of possible interventions. One of the strengths of our mechanistic ACED-HMM model is that we can consider possible changes or *interventions* to either the model parameters or assumptions about admissions. Below, we imagine two possible scenarios for the state of California, which chose to enact significant *restrictions* in late November and early December 2020 in light of rising hospital numbers and especially rising ICU utilization. After fitting our progression model to California count data, we forecast what would happen under two possible what-if scenarios. All forecasts were made with 30-x scaling.

We stress that we fit model parameters over counts between November 11th and January 11th (reusing an existing ABC fit for convenience), so the forecasts shown are to be interpreted as a *retrospective* analysis of what might have happened to the peak of the wave had the interventions considered been successfully deployed and extensively used. However, we emphasize that our method can also forecast into the *future* if desired.

What-if Scenario 1: Intervention that lowers hospitalization rates. Recent advances in pharmaceuticals have shown promising advances in monoclonal antibodies that might reduce hospitalizations (and deaths). A recent Phase 3 trial suggests that two drugs (bamlanivimab and etesevimab) together reduced hospitalizations and death by 87% when given to severely ill COVID-19 patients before they needed the hospital (Eil Lilly and Company, 2021). Suppose that policy makers were able to aggressively roll this treatment out over 30 days across the state of California, before the large wave of rising cases in late 2020. In Fig. 7, we show our model's fit to several scenarios: what actually happened (no reduction in admissions), an ideal retrospective rollout (a linear ramp up to a full 87% reduction in hospital admissions after 30 days), and two more realistic targets of a 50% and a 25% reduction. Given Fig. 7 plus knowledge of capacity limits, policy makers could use such quantitative forecasts to decide which rollout strategies to prioritize.

What-if Scenario 2: Pharmaceutical that lowers recovery times in the hospital. We next consider an intervention that changes the *number of days* spent when recovering in the hospital, motivated by a promising new treatment possibility. A recent clinical trial described by Beigel et al. (2020) suggests that the drug remdesivir reduced time to recovery from a median of 15 days (placebo) to a median of 10 days (treatment) for hospitalized patients with advanced cases of COVID-19. The study also reported a similar improvement among patients with severe disease, with recovery time reduced from a median of 18 days to a median of 11 days. We thus consider a scenario that assumes a 25% reduction in *recovery time*, as this would be a conservative assessment of such a therapy.

To operationalize this intervention in our model, for each segment ℓ of patient n's trajectory, we impose a 25% reduction in the sampled duration $\Delta_{n\ell}$ when the patient is recovering (when health indicator $h_{n\ell} = 1$). Durations in the model's declining health states are not modified. When we reduce durations, we round up or down to an integer number of days in a probabilistic way that preserves the expected value (e.g. if the scaled duration is 9.75, we return 10.00 75% of the time and 9.00 25% of the time). We further adjust to account for the fact that stays of length one cannot be reduced further.

Fig. 8 shows the difference between the standard and 25% reduction in recovering durations. As expected, we see noticable differences in the populations in the general ward.

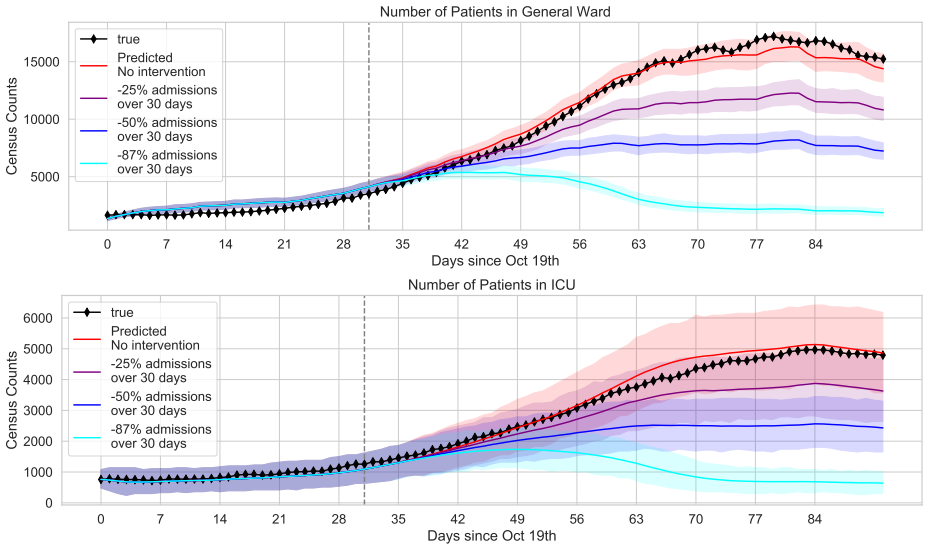

Figure 7: **Forecasted demand for General Ward (top) and ICU (bottom) beds in California under Scenario 1 (Sec. 6.6).**

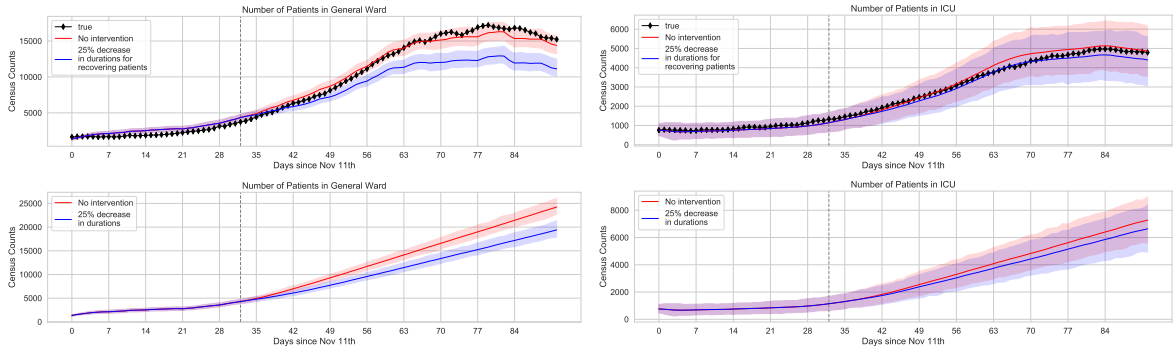

Figure 8: **Forecasted demand for General Ward beds (left) and ICU beds (right) using actual future counts (top) and a worst-case projection of counts (bottom) in California under What-if Scenario 2 (Sec. 6.6).**

However, the model suggests the ICU counts would not change much (probably because the ICU is unfortunately dominated by *declining* rather than *recovering* patients).

7. Discussion

We have contributed a new probabilistic model, developed a scalable ABC algorithm to draw samples from the (approximate) posterior distribution over model parameters, and validated these contributions on several datasets relevant to hospital demand modeling.

Limitations. Our proposed ACED-HMM model has several limitations. A major one is that it assumes the availability of admission counts when making forecasts, when of course for a real forecast into the future these counts are not known. We hope in future work to explore integrating models for forecasting future admissions, such as the model used by Qian et al. (2020). Another major limitation is that we currently assume that the values

of most parameters are static over time. In reality, we know that many factors are all changing over time, including properties of the disease (e.g. variants with different infection dynamics), characteristics of the infected population (e.g. age distributions), and hospital care practices. In the language of statistics, we know the real progression of patients through the hospital is neither *homogenous* nor *Markov*, so we should not expect our forecasts to be accurate far into the future. We could allow the model to *learn* how recovery probabilities or duration distributions might change over time. Finally, our model would likely be improved by capturing age as a key prognostic covariate that informs both the recovery probabilities and the duration probabilities. Naturally this would require more information, such as estimates of the age distribution on each day in the target region. However, if available this information could increase the model's power as an explanatory tool.

Further limitations can be ascribed to our proposed ABC methodology. Though our ABC procedure is simple and scalable, it is inefficient in the way it proposes samples via a random walk, with rather high rejection rates. In the future, we may consider Hamiltonian ABC (Meeds et al., 2015) methods to use *gradient* information to improve proposals and accelerate posterior exploration.

Advantages. Towards our twin goals of being able to provide reasonable forecasts and assess societal value, the *extreme portability* of our approach is a key advantage. The model requires only daily count data that are available from public health agencies throughout the world. There is no requirement for patient-level data. We further emphasize that the model and learning procedures are easily extended. Changing the model (such as adding age-dependent duration probabilities) would simply require editing the simulation code that generates a patient's sequential trajectory of states $z_{n,1:L_n}$ and durations $\Delta_{n,1:L_n}$, and specifying relevant prior and proposal distributions for any additional parameters.

Overall, we hope this study and our open-source code release leads to an improved ability to make hospital demand forecasts that are portable (by requiring only aggregate count data), interpretable and extrapolate-able (by using a mechanistic model), accurate (by fitting model parameters to local conditions via our ABC algorithm), and appropriately uncertain (by producing posterior distributions rather than point estimates). Although further work is needed to properly assess the societal value of possible interventions with this model, we believe our work represents a promising first step.

Acknowledgements

Authors GMV, CN, JTC, and MCH gratefully acknowledge funding support from a consortium of industry partners for this project – AstraZeneca, Bristol-Myers Squibb, Eli Lilly, Gilead Sciences, Janssen, Merck, Pfizer, and Regeneron – via an agreement with the Center for the Evaluation of Value and Risk in Health (CEVR) at Tufts Medical Center.

Authors MCH and DMK thank the Office of the Vice Provost for Research at Tufts University for support for this project under a "Tufts Springboard" award.

We thank Jinny Park (RA at Tufts Medical Center) for early assistance with literature surveys.

We thank several other graduate students in the Tufts Dept. of Computer Science who assisted with various early efforts on this project: Preetish Rath, Zhe Huang, and Panos

Lymperopoulos (early model prototyping efforts) as well as Gabriel Appleby, Diana Eastman, and Ab Mosca (visualization efforts).

References

S. Ahamad, S. Branch, S. Harrelson, M. K. Hussain, M. Saquib, and S. Khan. Primed for global coronavirus pandemic: Emerging research and clinical outcome. *European Journal of Medicinal Chemistry*, 209:112862, 2021.

C. Andrieu, N. De Freitas, A. Doucet, and M. I. Jordan. An introduction to MCMC for machine learning. *Machine Learning*, 50(1-2):5–43, 2003.

M. A. Beaumont. Approximate Bayesian Computation in Evolution and Ecology. *Annual Review of Ecology, Evolution, and Systematics*, 41(1):379–406, 2010. https://doi.org/10.1146/annurev-ecolsys-102209-144621.

M. A. Beaumont, W. Zhang, and D. J. Balding. Approximate Bayesian Computation in Population Genetics. *Genetics*, 162(4), 2002. https://www.genetics.org/content/162/4/2025.

C. Beckham and C. Pal. Unimodal probability distributions for deep ordinal classification. In *International Conference on Machine Learning*, 2017. http://proceedings.mlr.press/v70/beckham17a.html.

J. H. Beigel, K. M. Tomashek, L. E. Dodd, A. K. Mehta, B. S. Zingman, A. C. Kalil, E. Hohmann, H. Y. Chu, A. Luetkemeyer, et al. Remdesivir for the Treatment of Covid-19 — Final Report. *New England Journal of Medicine*, 383(19):1813–1826, 2020.

M. G. B. Blum and V. C. Tran. HIV with contact tracing: A case study in approximate Bayesian computation. *Biostatistics*, 11(4):644–660, 2010.

U. S. CDC. COVID-19 Pandemic Planning Scenarios. Technical report, U. S. Centers for Disease Control, 2020. https://www.cdc.gov/coronavirus/2019-ncov/hcp/planning-scenarios.html#table-2.

P. Chen, A. Nirula, B. Heller, R. L. Gottlieb, J. Boscia, J. Morris, G. Huhn, J. Cardona, B. Mocherla, et al. SARS-CoV-2 Neutralizing Antibody LY-CoV555 in Outpatients with Covid-19. *New England Journal of Medicine*, 384(3):229–237, 2021.

S. E. Congly, R. A. Varughese, C. E. Brown, F. M. Clement, and L. Saxinger. Treatment of Moderate to Severe Respiratory COVID-19—A Cost-Utility Analysis. *medRxiv*, 2020. https://www.medrxiv.org/content/10.1101/2020.09.21.20199182v2.

K. Cranmer, J. Brehmer, and G. Louppe. The frontier of simulation-based inference. *Proceedings of the National Academy of Sciences*, 117(48), 2020. https://www.pnas.org/content/117/48/30055.

Eil Lilly and Company. Lilly's bamlanivimab and etesevimab together reduced hospitalizations and death in Phase 3 trial for early COVID-19. 2021.

https://investor.lilly.com/news-releases/news-release-details/lillys-bamlanivimab-and-etesevimab-together-reduced.

R. H. Epstein and F. Dexter. A Predictive Model for Patient Census and Ventilator Requirements at Individual Hospitals During the Coronavirus Disease 2019 (COVID-19) Pandemic: A Preliminary Technical Report. *Cureus*, 12(6), 2020.

J. D. Ferguson. Variable duration models for speech. In *Proceedings of the Symposium on the Application of Hidden Markov Models to Text and Speech*, Princeton, NJ, USA, 1980.

S. Flaxman, S. Mishra, A. Gandy, H. J. T. Unwin, T. A. Mellan, H. Coupland, C. Whittaker, H. Zhu, T. Berah, et al. Estimating the effects of non-pharmaceutical interventions on COVID-19 in Europe. *Nature*, 584(7820):257–261, 2020.

J. Friedman, P. Liu, E. Gakidou, and I. C. M. C. Team. Predictive performance of international COVID-19 mortality forecasting models. *medRxiv*, page 2020.07.13.20151233, 2020.

A. Gandjour. How Many Intensive Care Beds are Justifiable for Hospital Pandemic Preparedness? A Cost-effectiveness Analysis for COVID-19 in Germany. *Applied Health Economics and Health Policy*, 19(2):181–190, 2021.

A. Gelman, J. B. Carlin, H. S. Stern, D. B. Dunson, A. Vehtari, and D. B. Rubin. *Bayesian Data Analysis*. CRC Press, 2013.

Y. Gu. Concerns with the IHME Model, 2020. https://covid19-projections.com/about/#concerns-with-the-ihme-model.

M. D. Hoffman and A. Gelman. The No-U-Turn Sampler: Adaptively Setting Path Lengths in Hamiltonian Monte Carlo. *Journal of Machine Learning Research*, page 31, 2014. http://jmlr.org/papers/volume15/hoffman14a/hoffman14a.pdf.

IHME COVID-19 Forecasting Team. Supplementary Information: Modeling COVID-19 scenarios for the United States. Supplementary Material, Nature Medicine, 2020. https://doi.org/10.1038/s41591-020-1132-9.

J. P. Ioannidis, S. Cripps, and M. A. Tanner. Forecasting for COVID-19 has failed. *International Journal of Forecasting*, 2020.

N. P. Jewell, J. A. Lewnard, and B. L. Jewell. Predictive Mathematical Models of the COVID-19 Pandemic: Underlying Principles and Value of Projections. *JAMA*, 323(19): 1893–1894, 2020.

Y. Jo, L. Jamieson, I. Edoka, L. Long, S. Silal, J. R. C. Pulliam, H. Moultrie, I. Sanne, G. Meyer-Rath, et al. Cost-effectiveness of remdesivir and dexamethasone for COVID-19 treatment in South Africa. *medRxiv: The Preprint Server for Health Sciences*, 2020.

D. Koeckerling, J. Barker, N. L. Mudalige, O. Oyefeso, D. Pan, M. Pareek, J. P. Thompson, and G. A. Ng. Awake prone positioning in COVID-19. *Thorax*, 75(10):833–834, 2020.

A. H. Lee, P. Lymperopoulos, J. T. Cohen, J. B. Wong, and M. C. Hughes. Forecasting COVID-19 Counts at a Single Hospital: A Hierarchical Bayesian Approach. In *ICLR 2021 Workshop on Machine Learning for Preventing and Combating Pandemics*, 2021. https://arxiv.org/abs/2104.09327.

M. L. Li, H. T. Bouardi, O. S. Lami, N. Trichakis, M. F. Zarandi, and D. Bertsimas. Overview of DELPHI Model V3. Technical report, COVIDAnalytics, 2020. https://covidanalytics.io/DELPHI_documentation_pdf.

J.-M. Marin, P. Pudlo, C. P. Robert, and R. J. Ryder. Approximate Bayesian computational methods. *Statistics and Computing*, 22(6):1167–1180, 2012. https://doi.org/10.1007/s11222-011-9288-2.

P. Marjoram, J. Molitor, V. Plagnol, and S. Tavaré. Markov chain Monte Carlo without likelihoods. *Proceedings of the National Academy of Sciences*, 100(26), 2003. https://www.pnas.org/content/100/26/15324.

E. Meeds, R. Leenders, and M. Welling. Hamiltonian ABC. *arXiv:1503.01916 [cs, q-bio, stat]*, 2015. http://arxiv.org/abs/1503.01916.

N. Metropolis, A. W. Rosenbluth, M. N. Rosenbluth, A. H. Teller, and E. Teller. Equation of State Calculations by Fast Computing Machines. *The Journal of Chemical Physics*, 21 (6):1087–1092, 1953.

C. D. Mitchell and L. H. Jamieson. Modeling duration in a hidden Markov model with the exponential family. In *1993 IEEE International Conference on Acoustics, Speech, and Signal Processing*, volume 2, pages 331–334, 1993.

C. J. Murray, others, and the IHME COVID-19 health service utilization forecasting team. Forecasting the impact of the first wave of the COVID-19 pandemic on hospital demand and deaths for the USA and European Economic Area countries. *medRxiv*, 2020. https://www.medrxiv.org/content/10.1101/2020.04.21.20074732v1.

P. J. Neumann, J. T. Cohen, D. D. Kim, and D. A. Ollendorf. Consideration Of Value-Based Pricing For Treatments And Vaccines Is Important, Even In The COVID-19 Pandemic. *Health Affairs*, 40(1):53–61, 2020.

Z. Qian, A. M. Alaa, and M. van der Schaar. CPAS: The UK's national machine learning-based hospital capacity planning system for COVID-19. *Machine Learning*, pages 1–21, 2020.

R. C. Reiner, R. M. Barber, J. K. Collins, P. Zheng, C. Adolph, J. Albright, C. M. Antony, A. Y. Aravkin, S. D. Bachmeier, et al. Modeling COVID-19 scenarios for the United States. *Nature Medicine*, 27(1):94–105, 2021.

M. Roimi, R. Gutman, J. Somer, A. Ben Arie, I. Calman, Y. Bar-Lavie, U. Gelbshtein, S. Liverant-Taub, A. Ziv, et al. Development and validation of a machine learning model predicting illness trajectory and hospital utilization of COVID-19 patients-a nationwide study. *Journal of the American Medical Informatics Association: JAMIA*, 2021.

J. Salvatier, T. V. Wiecki, and C. Fonnesbeck. Probabilistic programming in Python using PyMC3. *PeerJ Computer Science*, 2:e55, 2016.

The Atlantic Monthly Group. The COVID tracking project - Data API, 2021. https://covidtracking.com/data/api.

U. S. Dept. of Health and Human Services. COVID-19 reported patient impact and hospital capacity by state timeseries, 2021. https://healthdata.gov/Hospital/COVID-19-Reported-Patient-Impact-and-Hospital-Capa/g62h-syeh.

M. J. Wainwright and M. I. Jordan. Graphical Models, Exponential Families, and Variational Inference. *Foundations and Trends® in Machine Learning*, 1(1–2):1–305, 2008.

G. E. Weissman, A. Crane-Droesch, C. Chivers, T. Luong, A. Hanish, M. Z. Levy, J. Lubken, M. Becker, M. E. Draugelis, et al. Locally Informed Simulation to Predict Hospital Capacity Needs During the COVID-19 Pandemic. *Annals of Internal Medicine*, 2020.

S.-Z. Yu. Hidden semi-Markov models. *Artificial Intelligence*, 174(2):215–243, 2010.

J. Zhang, B. Xie, and K. Hashimoto. Current status of potential therapeutic candidates for the COVID-19 crisis. *Brain, Behavior, and Immunity*, 87:59–73, 2020.

D. Zou, L. Wang, P. Xu, J. Chen, W. Zhang, and Q. Gu. Epidemic Model Guided Machine Learning for COVID-19 Forecasts in the United States. *medRxiv*, page 2020.05.24.20111989, 2020.

Appendix A. Datasets

In our public code release, we include CSV files of the datasets we used for both the US and UK. Below, we describe how we obtained and preprocessed this data from original sources.

A.1. U.S. data.

Data representing state-level counts came from the U. S. Dept. of Health and Human Services (2021) and the Covid Tracking Project (CTP, The Atlantic Monthly Group (2021))[6]. We accessed the data in February 2021. These sources provide data for all 50 states, we selected a subset of states of interest: California (CA), Massachusetts (MA), South Dakota (SD), and Utah (UT). HHS data provided daily counts of hospital admissions and general ward occupancy counts (stage **G**), while CTP data provided ICU counts (**I** and **V**), as well as deaths (stage **T**).

As much as possible, we validated the consistency of these 2 public data sources by assuring that these counts matched with available corresponding data provided directly by state government public health agencies. For example, we verified the MA data matched counts released by the Massachusetts Department of Public Health[7].

In summary, our US predictive models all use standardized counts representing adult hospitalizations for *confirmed* COVID-19 cases. We are certain that our data for the general ward (**G**) accounts for the adult population while excluding pediatric cases. Through data-consistency checks across the 2 data sources, we convinced ourselves that CTP's **I**, **V**, and **T** data can be assumed as a good representation of adult populations (even though CTP reports uncertainty about whether their numbers include pediatric cases).

HHS fields used. HHS data descriptions are found on the clickable columns of the data web page[8]. We used the following data fields, with quoted definitions extracted from the data source.

- **previous day admission adult covid confirmed** : "Number of patients who were admitted to an adult inpatient bed on the previous calendar day who had confirmed COVID-19 at the time of admission in this state" (We considered previous day admissions as a feasible current day admission because admissions rates were not abruptly changing in orders of magnitudes between days. We recommend considering making the 1 day adjustment in future use of this data field.)
- **total adult patients hospitalized confirmed covid** : "Reported patients currently hospitalized in an adult inpatient bed who have laboratory-confirmed COVID-19. This include those in observation beds"
- **staffed icu adult patients confirmed covid** : "Reported patients currently hospitalized in an adult ICU bed who have confirmed COVID-19 in this state"

6. https://api.covidtracking.com/v1/states/daily.csv
7. https://www.mass.gov/info-details/archive-of-covid-19-cases-in-massachusetts
8. https://healthdata.gov/Hospital/COVID-19-Reported-Patient-Impact-and-Hospital-Capa/g62h-syeh/data

CTP fields used. CTP data descriptions are found in the 'historic values for all states' section of the data API webpage page[9]. We used the following data fields, with quoted definitions extracted from the data source.

- **inIcuCurrently** : "Individuals who are currently hospitalized in the Intensive Care Unit with COVID-19. Definitions vary by state / territory, and it is not always clear whether pediatric patients are included in this metric. Where possible, we report patients in the ICU with confirmed or suspected COVID-19 cases"
- **onVentilatorCurrently** : "Individuals who are currently hospitalized under advanced ventilation with COVID-19. Definitions vary by state / territory, and it is not always clear whether pediatric patients are included in this metric. Where possible, we report patients on ventilation with confirmed or suspected COVID-19 cases."
- **deathIncrease** : "Daily increase in death, calculated from the previous day's value."

We note that as of 2021-04-14, the CTP website relates the following message: "*The COVID Tracking Project has ended all data collection as of March 7, 2021. These files are still available, but will only include data up to March 7, 2021. We'll be publishing research through May, and then we will—fully and accessibly—archive our work and be done.*"

Obtaining stage-specific counts from raw data fields.

- Counts for daily admissions to the general ward were obtained from field **previous day admission adult covid confirmed**.
- **G** : Daily counts for general ward occupancy were obtained from field **total adult patients hospitalized confirmed covid** subtracting field **staffed icu adult patients confirmed covid**
- **I** : Daily counts for ICU-off-ventilator were obtained from field **inIcuCurrently** subtracting field **onVentilatorCurrently**
- **V** : Daily counts for ICU-on-ventilator were obtained from field **onVentilatorCurrently**
- **T** : Daily counts obtained from field **deathIncrease**

Variable data granularity across states. Not all states report counts from all stages. For example, UT and CA only provide aggregate ICU counts, and thus do not distinguish between on and off the ventilator. We thus take the provided count as the sum of the two ICU stages $\mathbf{I}, \mathbf{V}$ of our model, and adapt our ABC accordingly to evaluate a distance on this combined stage.

Smoothing terminal counts. For all states, we find the daily counts for the terminal death stage **T** to be both noisy and unreliable due to human factors in the reporting process. In particular, the reported counts often drop to unrealistic values at or close to zero during holidays and weekends (e.g. in some states we observed zero deaths on Thanksgiving and Christmas). Thus, we *smooth* these counts by replacing each day's raw value with the centered moving average across 5 days, being careful to not leak test-counts information into the moving average of training counts.

9. https://covidtracking.com/data/api

A.2. UK data.

We selected two hospital sites in England, United Kingdom with consistent data availability and a large volume of cases. We used public data sourced from the UK National Health Service (NHS)[10], which provided the count of beds occupied by COVID-19 patients on each day at each hospital. We used the following data fields:

- mechanical ventilators used for covid patients ($\mathbf{V}$)
- total number of beds used for covid patients ($\mathbf{G} + \mathbf{I} + \mathbf{V}$)
- patients discharged from covid hospitalization ($\mathbf{R}$)
- patients admitted with covid
- patients diagnosed in-hospital with covid but who were not admitted as covid patients

In our experiments, we aggregated daily covid admissions and daily in-hospital covid diagnoses to form the daily admissions in $\mathbf{G}$ that are then fed into ACED-HMM. The two hospital sites we selected had the same available counts. Unlike for US data, we did not find the need to smooth any count.

Appendix B. Additional Results

B.1. Quantitative assessment: How accurate are the forecasted counts?

We next assess how *accurate* the forecasted counts are, in terms of mean absolute error from the observed counts in the test set. In Table B.1, we show mean absolute errors for our proposed ACED-HMM + ABC (averaged over all days in the forecasting period) for 3 US states. We further perform the same assessment on 2 single hospital sites from the UK in Table B.2.

On select datasets, we compare to several reasonable baselines. (We did not try all methods on all datasets due to limited computational resources and the expected poor performance of most baselines). First, we consider "ACED-HMM + Prior", which makes forecasts using the *prior* distribution over our model's parameters, rather than the posterior fit via ABC. This could indicate how reliable our model would be if we did not adapt parameters to the specific region of interest but instead chose values for transition and duration probabilities from a reasonable literature survey (as our prior is chosen). This could also indicate how important other factors (such as the provided admission counts in testing period) are to the forecast. Second, we compare to "AR-Poisson", a non-mechanistic probabilistic autoregressive model with a Poisson likelihood that forecasts each univariate count time-series individually, inspired by Lee et al. (2021). This is a custom univariate forecasting model fit to each stage separately. It does not use admission counts at all. See Appendix E for details.

For all U.S. states we compare against the January 15th public release of IHME model forecasts (Reiner et al., 2021). These forecasts were produced by the IHME team by training on data available before January 12th, thus matching the start of our testing period almost exactly. This model does not make use of admission counts from the testing period. See Appendix F for details.

10. https://www.england.nhs.uk/statistics/statistical-work-areas/covid-19-hospital-activity/

		G InGeneralWard			I + V InICU			V OnVentInICU			T sm. Death		
	Method	MAE	lower	upper	MAE	lower	upper	MAE	lower	upper	MAE	lower	upper
MA	ACED-HMM + ABC	65.0	61.5	68.9	15.7	14.5	16.9	34.0	32.6	35.7	8.0	7.8	8.3
	ACED-HMM + Prior	868.6	779.6	945.8	293.6	272.6	313.3	119.6	113.8	124.8	40.7	39.1	42.2
	AR-Poisson	498.0	438.3	553.6	162.2	148.6	173.5	128.3	118.5	138.6	34.8	28.4	42.0
	IHME	1066.1	*543.4	1754.9	104.0	*15.6	257.9	25.7	*41.4	106.5	21.6	*8.7	49.7
	Mean Test y	1141.6			392.5			249.1			66.5		
SD	ACED-HMM + ABC	9.2	8.5	10.1	4.5	4.3	4.8	4.8	4.5	5.1	2.8	2.7	2.9
	IHME	71.8	*6.6	166.4	17.7	*4.2	46.0	5.9	*6.3	20.6	2.5	*3.6	5.0
	Mean Test y	102.5			34.9			23.6			7.8		
UT	ACED-HMM + ABC	20.8	20.2	21.3	18.2	17.4	19.2	NA			2.4	2.3	2.5
	IHME	332.9	*142.6	578.4	105.0	*35.7	213.9	NA			7.4	*2.7	15.7
	Mean Test y	272.9			164.3			NA			11.7		

Table B.1: Quantitative error assessment on 3 U.S. states. We measure error on the testing period (Jan. 11 - Feb. 11, 2021) with respect to the observed counts at each possible care stage: general ward **G**, in ICU (including on and off ventilator) $\mathbf{I}+\mathbf{V}$, on ventilator in ICU **V**, and *smoothed* death counts **T** sm.). For all states and stages, we report the mean count y across the testing period to give a sense of scale. Cells marked NA were not available for that state (see discussion in App. A). AR-Poisson baseline is described in App. E, IHME baseline in App. F. We communicate uncertainty by reporting lower and upper estimates of the MAE. To obtain these intervals for all variants of our ACED-HMM as well as our AR-Poisson baseline, we repeat all MAE computations across 100 separate batches of posterior samples. We compute and report the 2.5th and 97.5th percentiles across these batches. For the IHME baseline, a distribution of forecasted samples is not available. Thus, we report the MAE computed using the mean estimate forecast, as well as the MAE computed using the provided lower and upper estimates count values. This second kind of interval (marked with *) should not be directly compared to the first, as they capture different aspects of uncertainty.

For both versions of ACED-HMM and for the autoregressive model, we compute the MAE and its confidence interval as follows. We draw 100 samples from the posterior (prior for ACED-HMM + Prior) distribution over the model parameters, we produce individual forecasts for each sample, and compute the MAE using the mean of these forecasts. We repeat the process 100 times, and we report the average MAE with the 2.5th - 97.5th percentile range across these batches as confidence interval. The public release of forecasts from IHME only provides three daily forecast values - a mean estimate, a lower bound and an upper bound - thus making it impossible to compute a confidence interval analogous to that which we compute for the other three models. Thus, we simply report the MAE computed using each of the three estimates. The IHME uncertainty intervals (marked with *) are given for completeness, but should be recognized as different from the other intervals and not directly compared.

B.2. Quantitative Assessment: Posterior Coverage

Below, we consider the *coverage* of the estimated posteriors produced by our procedure.

In Tab. B.3 and B.4, we show the 50%, 80% and 95% coverage fractions. Ideal probabilistic models that are well-calibrated would have an empirical fraction of observations *exactly equal to* the target fraction. However, fractions of observations *greater* than the target fraction are more desirable than those *lower*, as that indicates a better fit to the observations by the median of the forecasts. We see that all models could be better calibrated. However, our ACED-HMM trained with ABC has a great fit to the $\mathbf{G}+\mathbf{I}+\mathbf{V}$ counts and **V** counts on both UK hospitals, as well as a near-perfect fit to the $\mathbf{I}+\mathbf{V}$ counts on US states, counts

		$\mathbf{G}+\mathbf{I}+\mathbf{V}$	All Beds	$\mathbf{V}$	OnVentInICU	$\mathbf{R}$	Recovered
	Method	MAE	lower - upper	MAE	lower - upper	MAE	lower - upper
South Tees	ACED-HMM + ABC	8.7	7.7 - 10.2	4.6	3.9 - 5.1	5.7	5.5 - 5.8
	ACED-HMM + Prior	118.4	109.8 - 125.9	10.7	10.0 - 11.4	5.9	5.7 - 6.2
	AR-Poisson	49.2	40.3 - 60.5	417.3	15.8 - 2209.5	49.2	9.7 - 518.7
	Mean Test y	199.5		31.1		20.8	
Oxford	ACED-HMM + ABC	18.0	15.4 - 22.4	6.3	5.5 - 6.9	13.4	13.2 - 13.6
	Mean Test y	274.7		37.7		33.1	

Table B.2: Quantitative error assessment for predictions for two UK hospital sites during the testing period (Jan. 11 - Feb. 11, 2021). We assess mean absolute error (MAE) at each stage where we have available "ground-truth" count data for these sites: total hospital bed count $\mathbf{G}+\mathbf{I}+\mathbf{V}$, count of patients on ventilator in ICU $\mathbf{V}$, and counts of patients who recovered $\mathbf{R}$. For all sites and stages, we report the mean count y across the testing period to give a sense of scale. AR-Poisson baseline is described in App. E. We communicate uncertainty by reporting lower and upper estimates on the MAE, which we obtain by repeating all MAE computations across 100 separate batches of posterior samples. We compute and report the 2.5th and 97.5th percentiles across these batches.

that have been the metric most commonly used by US states' legislatures to determine the imposition of social-distancing measures. We wish to emphasize that coverages need to be put in the context of their MAEs as well. For instance, while ACED-HMM has worse 95% coverage than AR-Poisson on $\mathbf{G}$ counts, that is because AR-Poisson has much worse MAE with a very high uncertainty interval, effectively making AR-Poissons's predictions less useful than those of ACED-HMM. That being said, ACED-HMM appears to be too confident in its predictions. However, we note that the scalability approximation that we propose provides more conservative uncertainty estimates.

B.3. Synthetic Data Assessment: Can we recover "ideal" model parameters?

We assessed the ability of our procedure to recover "ideal" model parameters under different admissions regimes. We selected a set of parameters that deviated significantly, though not excessively from the prior we derived from CDC data. Then, we simulated sets of counts using these parameters and a fixed random seed under 4 admissions regimes, respectively with 1-x, 3-x, 6-x and 9-x the amounts of true admissions at South Tees Hospitals between November 3rd and February 3rd. We note that the 9-x admissions regime is comparable to that of Massachusetts in terms of total admitted patients, and it thus can be considered a regional-level regime. We then used ABC with the same prior to learn 5 sets of model parameters to fit each of the 5 simulated counts, respectively. We used all possible counts for training: $\mathbf{R}$, $\mathbf{G}$, $\mathbf{I}$, $\mathbf{V}$ and $\mathbf{T}$.

ABC was able to identify parameters that provided a close-to-optimal fit to the training counts as well as high-quality forecasts on test counts. While the parameters learned were optimal in their ability to explain the training data, in no case were they "ideal", i.e. the true parameters. In particular, we observed that, the higher the number of total admitted patients, the closer the learned parameters are to the true ones, as can be seen by comparing Fig. B.4 and Fig. B.5, which show the posterior distributions for the 1-x (hospital-level) and 9-x (regional-level) regimes, respectively. Under the regional-level regime, 5 parameters are fully recovered (i.e. mean of posterior matches true parameters), 2 parameters are partially recovered (i.e. posterior shifts from prior towards true parameter), 3 parameters are not

	Coverage (%)	G	I	V	I+V	T	T sm.
South Dakota	ACED-HMM + ABC *95*	87	77	81	100	45	77
	80	52	48	71	97	23	68
	50	42	26	32	55	6	32
Utah	ACED-HMM + ABC *95*	71	NA	NA	100	55	100
	80	39	NA	NA	100	32	87
	50	19	NA	NA	61	23	39
Massachusetts	AR-Poisson *95*	81	100	45	61	100	100
	80	45	90	26	35	68	87
	50	29	35	13	13	32	10
	ACED-HMM + Prior *95*	52	39	61	71	42	23
	80	6	35	42	39	26	23
	50	6	19	19	23	23	19
	ACED-HMM + ABC *95*	68	65	42	97	55	84
	80	48	45	16	94	39	74
	50	32	16	3	74	16	58

Table B.3: Coverage assessment for forecasts based on methods fit on U.S. state-level data. This metric assesses how reliably calibrated the forecasted *distributions* each method produces may be on future unseen data. Given many samples from a predicted distribution, we obtain a centered interval of specified coverage fraction by computing the relevant percentiles of the samples (e.g. for the 80% coverage fraction our interval is defined by the 10th to 90th percentiles). We report the observed fraction of daily count data within the testing period at each stage that fall within that predicted interval. Ideally, the observed fraction should be close to the intended coverage fraction.

recovered (i.e. no shift from prior towards true parameters).

Under our modeling assumptions, higher admissions regimes generate counts which are reproducible by fewer sets of parameters. In other words, the space of "optimal" parameters shrinks. Thus, on higher admissions regimes, our procedure converges closer to the true parameters.

Furthermore, we observed that certain parameters are easier to recover than others. For instance, parameters that have a direct effect on **R** and **T** counts seem to be among the first to be recovered, this includes the duration probabilities recovering in **G** and declining in **V**. By contrast, the parameters at the interface between hospital stages seem harder to recover.

We believe another useful experiment using synthetic data to be one that answers the question *How informative does the prior need to be for the posterior to recover all the "ideal" parameters?*. We leave the answering of this question for future work.

Appendix C. Details of Progression Model

C.1. View of our model as Hidden Markov Model

In the main paper, we discuss how our proposed model can be seen as an explicit duration hidden Markov model with 9 states: $\mathbf{S}, \mathbf{G}0, \mathbf{G}1, \mathbf{I}0, \mathbf{I}1, \mathbf{V}0, \mathbf{V}1, \mathbf{T}, \mathbf{R}$. We provide the transition matrix for this model in Table C.1.

	Coverage (%)		R	G+I+V	V
South Tees	AR-Poisson	*95*	90	100	100
		80	52	100	100
		50	3	58	74
	ACED-HMM + Prior	*95*	77	100	84
		80	58	13	42
		50	29	10	26
	ACED-HMM + ABC	*95*	77	100	97
		80	48	100	87
		50	26	97	39
Oxford	ACED-HMM + ABC	95	55	100	100
		80	19	100	77
		50	10	87	35

Table B.4: Coverage assessment for forecasts based on fits to two U.K. individual hospital sites. This metric assesses how reliably calibrated the forecasted *distributions* each method produces may be on future unseen data. Given many samples from a predicted distribution, we obtain a centered interval of specified coverage fraction by computing the relevant percentiles of the samples (e.g. for the 80% coverage fraction our interval is defined by the 10th to 90th percentiles). We report the observed fraction of daily count data within the testing period at each stage that fall within that predicted interval. Ideally, the observed fraction should be close to the intended coverage fraction.

prev. state \ next state	**R**	**G**1	**I**1	**V**1	**G**0	**I**0	**V**0	**T**
S		ρ_G			$1-\rho_G$			
G1	1							
I1	r_I	$1-r_I$						
V1	r_V		$1-r_V$					
G0			$\rho_I(1-d_G)$			$(1-\rho_I)(1-d_G)$		d_G
I0				$\rho_V(1-d_G)$			$(1-\rho_V)(1-d_I)$	d_I
V0								1

Table C.1: State transition probabilities assumed by the explicit-duration HMM equivalent of our model: rows correspond to the previous state and columns indicate possible next states. Blank entries all have zero probability, but are kept blank for visual clarity. It is not possible to transition into the start state **S** or out of the terminal states **R** and **T**, so these rows/columns are omitted.

C.2. Recovery probabilities

We reproduce the relevant numbers from the CDC's Table 2 in Table C.2, and then describe how these estimates are turned into a prior over ρ. We first convert these estimates to single, age-independent estimates by computing the average across age groups weighted by the US country-level age distribution of hospital patient provided by the CDC [11] during the week of November 7th. We show the computed average on the right-most column of Table C.2. Then, assuming fixed values for the probabilities of dying d and given these numbers, we derive the probability of recovering at each stage. Let $p(\mathbf{I})$ be the percent of patients transferred to the ICU, $p(\mathbf{V})$ the percentage of patients who receive ventilation, and $p(\mathbf{T})$ the percent of patients who die, we compute the mean the priors for $\rho_{\mathbf{G}}$, $\rho_{\mathbf{I}}$ and

11. https://gis.cdc.gov/grasp/covidnet/COVID19_3.html

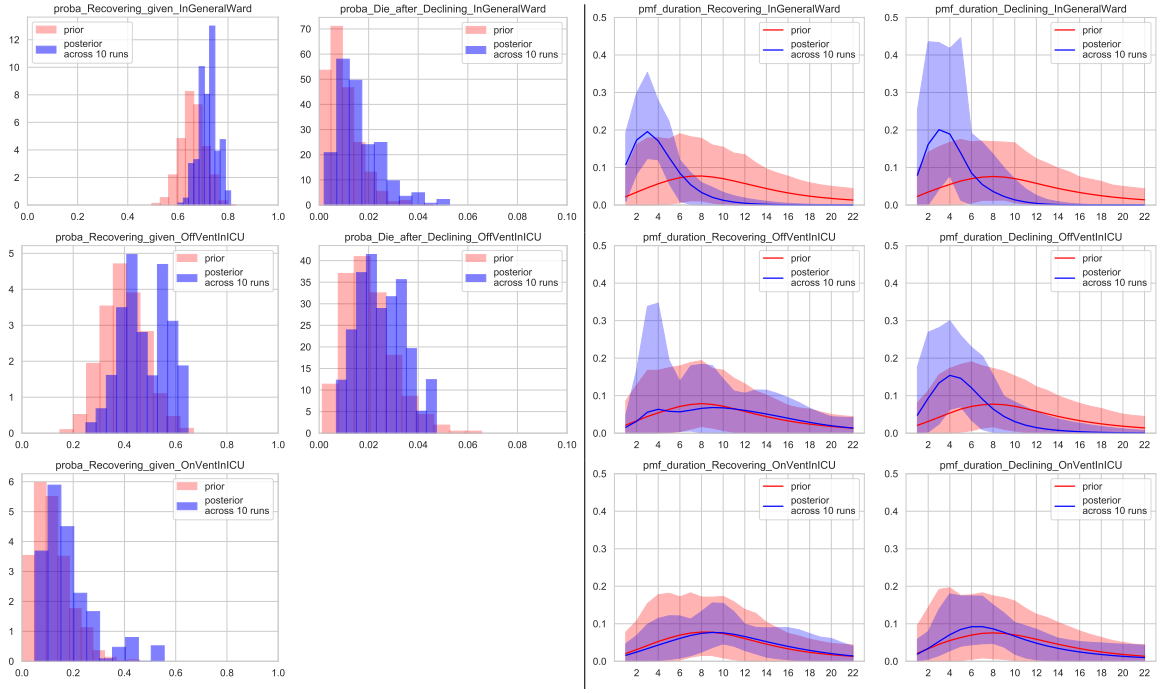

Figure B.1: **Posterior distributions over parameters for South Tees hospital in the UK (Nov. 3rd - Jan. 3rd).** We show transition parameters (left) and duration parameters (right) after fitting on 2 months of counts, where each day we used available census counts for $\mathbf{R}$, $\mathbf{G}+\mathbf{I}+\mathbf{V}$, and $\mathbf{V}$. The colored interval of duration plots shows the 2.5 - 97.5th percentile intervals of 2000 samples (10 runs, each with 200 samples). The prior is also shown for comparison.

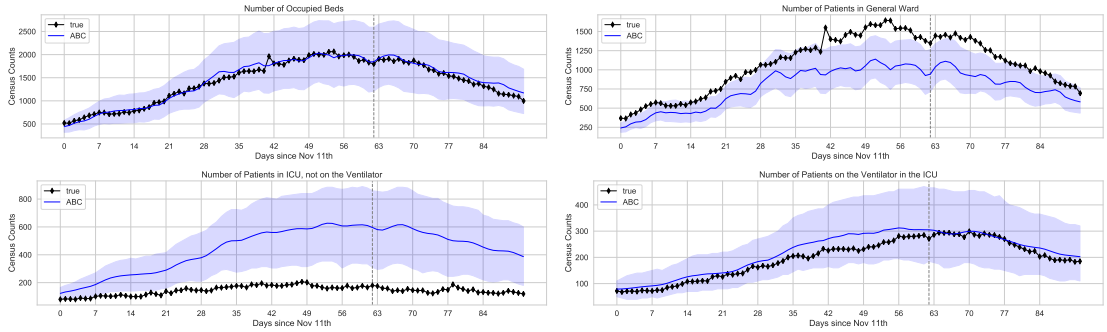

Figure B.2: **Fit and forecasts on MA data for ACED-HMM trained to match counts that combine multiple stages of care.** Here, the ACED-HMM was trained to match the total number of hospital beds ($\mathbf{G}+\mathbf{I}+\mathbf{V}$) as well as terminal counts ($\mathbf{T}$) for MA state-level data. (Compare to Fig. 3, which fit on counts for individual stages $\mathbf{G}$, $\mathbf{I}$, $\mathbf{V}$, and $\mathbf{T}$). The model is able to fit and forecast the total bed counts accurately (upper-left), but did not recover the counts at some individual compartments ($\mathbf{G}$: lower left, $\mathbf{I}$ upper right) well. The ventilator counts ($\mathbf{V}$: lower right) are near-optimally recovered as they have a very direct influence over the observed $\mathbf{T}$ counts.

$\rho_{\mathbf{V}}$ by solving for them in the following equations:

$$1 - p(\mathbf{I}) = \rho_{\mathbf{G}} + ((1 - \rho_{\mathbf{G}})d_{\mathbf{G}})$$
$$p(\mathbf{V}) = p(\mathbf{I})(1 - \rho_{\mathbf{I}})(1 - d_{\mathbf{I}})$$

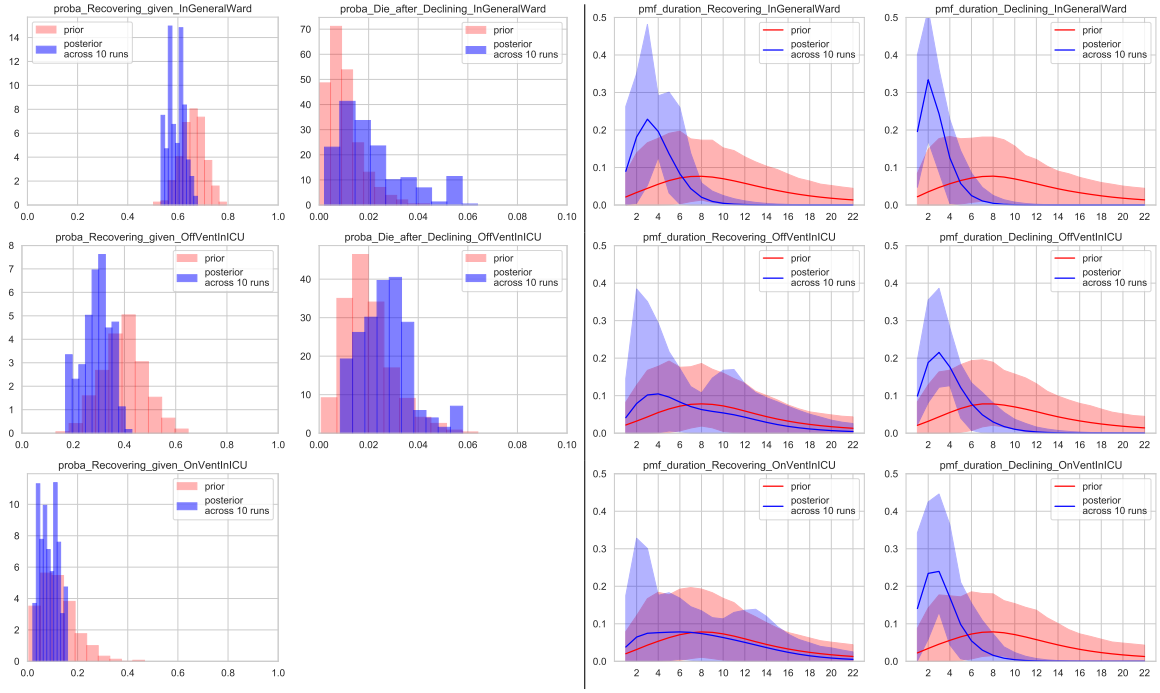

Figure B.3: **Posterior distributions over parameters for Massachusetts (Nov. 11th - Jan. 11th) using aggregate bed counts for training.** We show transition parameters (left) and duration parameters (right) after fitting on 2 months of counts, where each day we used census counts for $\mathbf{G}+\mathbf{I}+\mathbf{V}$, and $\mathbf{T}$. The colored interval of duration plots shows the 2.5 - 97.5th percentile intervals of 2000 samples (10 runs, each with 200 samples). The prior is also shown for comparison.

Age	18-49	50 - 64	65+	Avg.
Percent transfered to ICU	23.8	36.1	35.3	34.3
Percent who receive ventilation	12.0	22.1	21.1	20.4
Percent who die	2.4	10.0	26.6	19.3

Table C.2: Reproduced from Table 2 of CDC (2020), when accessed on March 19, 2021. We added the right-most column.

$$p(\mathbf{T}) = p(\mathbf{V})(1-\rho_{\mathbf{V}}) + p(\mathbf{I})(1-\rho_{\mathbf{I}})d_{\mathbf{I}} + d_{\mathbf{G}}$$

The found values for $\rho_{\mathbf{G}}$, $\rho_{\mathbf{I}}$ and $\rho_{\mathbf{V}}$ denote the ratios of parameters for the beta priors. To set the variance for the priors, we set the beta parameters for the prior over each ρ by multiplying ρ and $1-\rho$ by a scalar value r. For $\rho_{\mathbf{G}}$, we empirically set $r_{\mathbf{G}} = 100$. Then, we set $r_{\mathbf{I}} = r_{\mathbf{G}}(1-\rho_{\mathbf{G}})$ and $r_{\mathbf{V}} = r_{\mathbf{I}}(1-\rho_{\mathbf{I}})$. This increases the uncertainty in prior in proportion to the *influx* of patients in the different stages expected under the regime specified by the prior mean probabilities.

For both probabilities of death, we set $r = 200$ to indicate strong confidence in the low value that we set and discourage exploration towards unrealistic values.

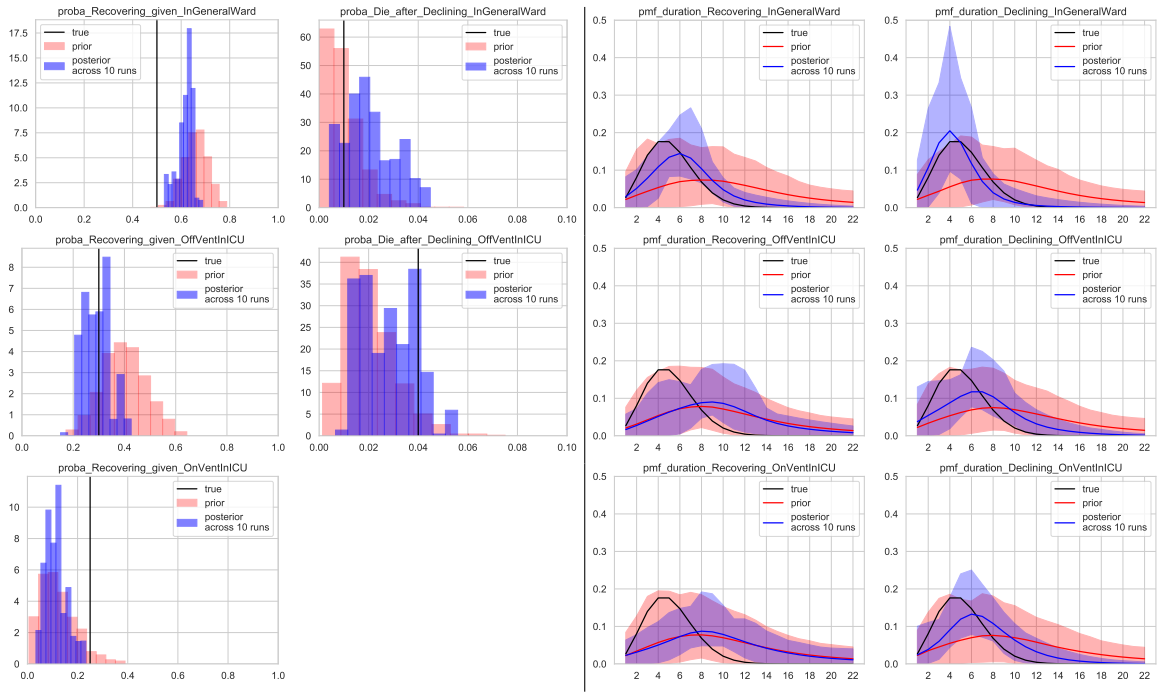

Figure B.4: **Posterior distributions over parameters for synthetic data with hospital-level admissions.** We show transition parameters (left) and duration parameters (right) after fitting on 61 days of counts, where each day we used available simulated census counts for $\mathbf{R}, \mathbf{G}, \mathbf{I}, \mathbf{V}$, and $\mathbf{T}$. The colored interval of duration plots shows the 2.5 - 97.5th percentile intervals of 2000 samples (10 runs, each with 200 samples). The prior is also shown for comparison.

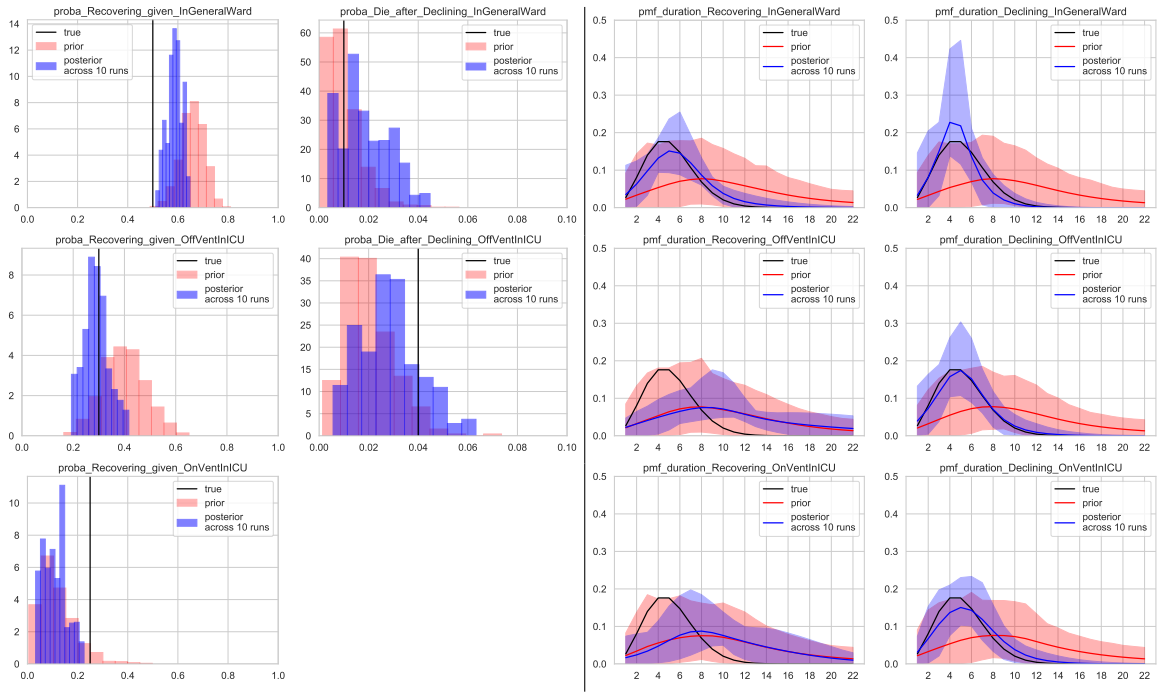

Figure B.5: **Posterior distributions over parameters for synthetic data with regional-level admissions.** We show transition parameters (left) and duration parameters (right) after fitting on 61 days of counts, where each day we used available simulated census counts for $\mathbf{R}, \mathbf{G}, \mathbf{I}, \mathbf{V}$, and $\mathbf{T}$. The colored interval of duration plots shows the 2.5 - 97.5th percentile intervals of 2000 samples (10 runs, each with 200 samples). The prior is also shown for comparison.

Appendix D. Details of ABC Learning Procedure

Biasing the distance computation. For every dataset, we set weight u_k for each count type k such that counts that are generated at stages farther away from admissions are worth more, and such that their average is 1.0, so that the upper bound on the distance is preserved at 1.0. The rationale behind this is that counts generated farther away from admissions are generally harder to recover, as indicated by the greater uncertainty of ABC in predicting those counts that we see in our experiments.
For MA and SD, where $\mathbf{G}, \mathbf{I}, \mathbf{V}$ and $\mathbf{T}$-smoothed counts are available, we set $u_{\mathbf{G}} = 0.7$, $u_{\mathbf{I}} = 0.9$, $u_{\mathbf{V}} = 1.1$ and $u_{\mathbf{T}} = 1.3$. For UT and CA, where $\mathbf{G}, \mathbf{I}+\mathbf{V}$ and $\mathbf{T}$-smoothed counts are available, we set $u_{\mathbf{G}} = 0.8$, $u_{\mathbf{I}+\mathbf{V}} = 1.0$ and $u_{\mathbf{T}} = 1.2$. For the data ablation experiment on MA, we set $u_{\mathbf{G}+\mathbf{I}+\mathbf{V}} = 0.8$ and $u_{\mathbf{T}} = 1.2$. For both UK hospitals, we set $u_{\mathbf{R}} = 0.8$, $u_{\mathbf{G}+\mathbf{I}+\mathbf{V}} = 1.0$ and $u_{\mathbf{T}} = 1.2$. For the experiments on synthetic data, we set $u_{\mathbf{G}} = 0.8$, $u_{\mathbf{R}} = 0.9$, $u_{\mathbf{I}} = 1.0$, $u_{\mathbf{V}} = 1.1$ and $u_{\mathbf{T}} = 1.2$.

Justification of the maximum-normalized distance computation. At an individual timestep t, we assess distance via a mean absolute error normalized by the maximum between individual entries (which keeps this value on a unit scale). A side-effect of this normalization is that parameters that overestimate the true counts are preferred over parameters that underestimate the true counts by the same margin. For example, if true count $y_t^k = 20$ and simulated count $\tilde{y}_t^k = 22$, then the relevant distance will be $\frac{|20-22|}{22} = \frac{1}{11}$. Instead, if $\tilde{y}_t^k = 18$, the relevant unweighted portion of the distance will be $\frac{|20-18|}{20} = \frac{1}{10}$. This asymmetry enforces a pessimistic bias that in our experimental circumstances would be appropriate - e.g., when developing forecasts that will be used to determine what resources a hospital will need to meet future demand. In any case, the scheme at most moderately favors over prediction of utilization, compared to under utilization. Alternative distances could be easily considered.

Scheduling the decay. We draw samples from a *burn-in* phase and a *sampling* phase. During the *burn-in* phase, we anneal ε across iterations with the goals of 1) making it converge to an optimal value for sampling, and 2) dragging the parameters to the high-density region of the parameter space. Then, during the *sampling* phase, we stop the annealing, and draw samples in standard ABC MCMC as described in Marjoram et al. (2003), where ε is held fixed across iterations.
Crucially, in the sampling phase, we raise ε by a small value compared to the best value found during the burn-in phase, so that we accept slightly more diverse samples than it would have otherwise.

In the *burn-in* phase, we anneal ε in the following way. The upper-bound on our distance d allows us to initialize ε to 1.0. In practice, we find that ε can often be safely initialized to a lower value, thus reducing the number of iterations needed for convergence. We anneal ε exponentially after each parameter proposal using hyperparameter γ. Crucially, we never allow ε to take a value below the last accepted distance d_{best}, thus allowing the algorithm to naturally converge to a value of ε that is optimal for sampling, as it is low enough that most proposals get rejected for not being able to provide a better match to the training data. We apply one more change to the annealing schedule: at regular intervals during the *burn-in* phase, we increase ε by a fixed value p. This allows the algorithm to "escape" a local optima

that might have been encountered along the way. We found this to be particularly useful for fitting parameters to datasets containing fewer patients, such as single-hospital datasets. Indeed, with fewer patients to model, the variance in the counts generated by a given set of parameters is higher, thus it is more likely that a given set of proposed parameters gets accepted due to a particularly "lucky" simulation, which had assigned an unusually low distance to the proposed parameters.

Specific tuning of the decay schedule. In all our experiments, we initialize ε to 0.7, as we find such value to be always greater than the distance generated using samples from the prior. We fix the number of *burn-in* iterations to 24,000 (where one iteration makes and evaluates a proposal for each of the 17 parameters in turn, for a total of 408,000 total single-parameter iterations), p to 0.05, and f to 0.15. To set the annealing parameter γ, we consider the following. The optimal, convergence value of ε varies by dataset. In particular, due to the design of our distance function, datasets with higher counts have a lower convergence value. An approximate lower bound to the convergence value can be quickly found for any dataset by computing the average distance between multiple sets of counts generated with the dataset's admissions and a fixed set of parameters, and a single representative of such counts. Though our annealing schedule is designed to be likely to escape local optima, we find it desirable, especially for lower-counts datasets, to set γ such that ε does not excessively undershoot the approximate lower bound by the end of the training iterations. Concretely, this translates to lower-counts datasets having higher γ, and thus slower annealing, in our experiments.

Details of proposal distributions. For each transition probability τ_k, we propose a new value τ_k^* by sampling from a Beta distribution whose mean is the old value and with a scaling parameter $r > 0$ that determines the variance: $\tau_k^* \sim \text{Beta}(r\tau_k, r(1-\tau_k))$. We set $r = 100$ for the recovering probabilities and to $r = 200$ (lower entropy) for death probabilities.

For the mode of each duration probability $\lambda^{s,h}$, we propose a new value $\lambda^{*s,h}$ by sampling from a truncated normal distribution with mean at $\lambda^{s,h}$ and a variance of 0.25: $\lambda^{*,s,h} \sim \text{TruncNorm}(\lambda^{s,h}, 0.25, [1, D])$. For the *log* of each temperature parameter $\nu^{s,h}$, we sample a new value from a normal distribution centered at the old value, with a variance of 0.01: $\nu^{*s,h} \sim \text{Norm}(\nu^{s,h}, 0.01)$.

Warm start. At the start of the simulated training period, it is unrealistic to assume that the initial patients in each hospital stage have only just been admitted to said stage (i.e. they are all at day zero of their stay). Thus, in an effort to more realistically model the progression through the hospital of the initial population, we apply a simple 'warm start' heuristic, in which we simulate the admission of the initial population in each state by uniformly distributing them during 5 days previous to day zero. We increase the admissions by 3% in both G and V to account for any patients who exit the hospital before the official start of the training period.

Details of ensembling. For all experiment, we collect 200 samples each from 10 different runs of the algorithm, resulting in 2000 total samples. We only use runs which we have verified to have converged to similar values of ε, and thus produce samples that explain the training counts equally well.

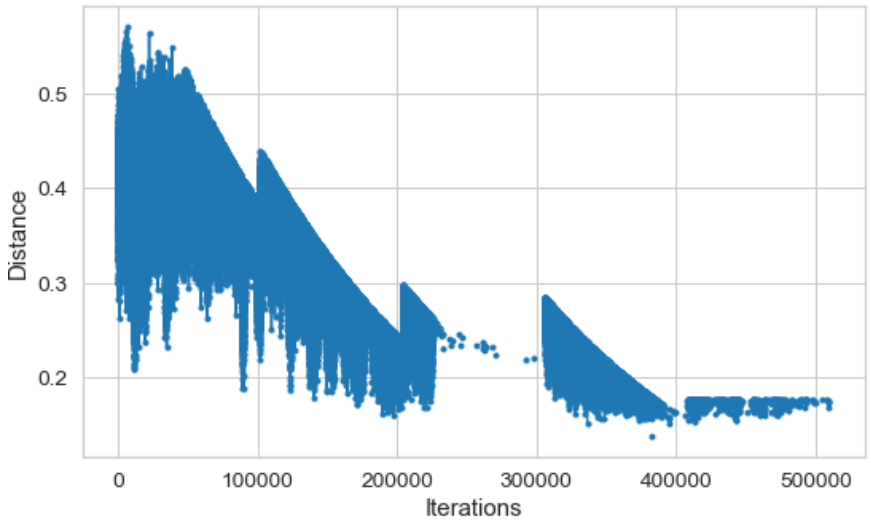

Figure D.1: **Trend of accepted distanced on one run of ABC for ACED-HMM on South Tees hospital data.** Each data point indicates a set of parametrs that has surpassed the first stage of acceptance (distance below ε). Around iteration 230,000 the algorithm got stuck in a local optimum, where few proposals were getting accepted. The resetting of ε after iteration 300,000 helped the algorithm get unstuck from the local optimum.

Appendix E. Details of Baseline Autoregressive-Poisson forecasting model

We consider a simple probabilistic model for univariate counts, the *latent autoregressive Poisson* or just AR-Poisson for short.

Model Setup. Suppose across T days we observe a univariate time series $y_{1:T} = [y_1, y_2, \dots y_T]$, where $y_t \in \{0, 1, 2, \dots\}$ indicates the count of patients in a particular stage on day t. Our goal is to develop *forecasts* for the next F days, given all previous observations, using a conditional probabilistic model $p(y_{(T+1):(T+F)} \mid y_{1:T})$.

We consider an order-1 autoregressive process as our latent variable model, where each timestep has a latent real value $f_t \in \mathbb{R}$. We capture dependency across time in the latent series $f_{1:T}$, and model each count y_t as conditionally independent given f_t:

$$p(f_{1:T}, y_{1:T}) = \prod_{t=1}^{T} p(f_t \mid f_{t-1}) \cdot \prod_{t=1}^{T} p(y_t \mid f_t). \tag{8}$$

For most timesteps $t > 1$, we generate the latent value f_t using the previous value f_{t-1}:

$$p(f_t \mid f_{t-1}) = \text{Normal}(\beta_0 + \beta_1 f_{t-1}, \sigma^2), \ t \in 2, 3, \dots \tag{9}$$

The very first value f_1 is generated with mean β_0:

$$p(f_1) = \text{Normal}(\beta_0, \sigma^2) \tag{10}$$

The latent-generating parameters are coefficient vector $\beta = [\beta_0, \beta_1]$ and standard deviation $\sigma > 0$.

We then generate each observed count y_t using a Poisson likelihood, setting the mean parameter by transforming the latent f_t to a positive value via the exponential:

$$p(y_t \mid f_t) = \text{Poisson}(\exp(f_t)). \tag{11}$$

Forecasting Method. We wish to first sample from the posterior over parameters β, σ, and latent values f: $p(\beta, \sigma, f_{1:T} \mid y_{1:T})$. We place the follow vague priors over the parameters:

$$\beta_0 \sim \text{Normal}(0, 0.1), \tag{12}$$

$$\beta_1 \sim \text{Normal}(1, 0.1), \tag{13}$$

$$\sigma \sim \text{HalfNormal}(0.1). \tag{14}$$

We then use the No-U-Turn sampler (Hoffman and Gelman, 2014) to perform Markov chain Monte Carlo approximation of the posterior. Our NUTS sampler is implemented using the PyMC3 toolbox (Salvatier et al., 2016).

Given a single posterior sample indexed by s, with parameters β^s, σ^s and latents $f^s_{1:T}$, we can then use the generative model to draw a *forecast* of latents f and counts y for the next F days:

$$f^s_{T+\tau} \sim \text{Normal}(\beta^s_0 + \beta^s_1 f^s_{T+\tau-1}, \sigma^s), \qquad \tau \in 1, \dots F \tag{15}$$

$$y^s_{T+\tau} \sim \text{Poisson}(\exp(f^s_{T+\tau})), \qquad \tau \in 1, \dots F \tag{16}$$

We typically draw a forecast of S distinct samples, using $S = 1000$ or more to be sure we're capturing the full distribution.

Results. In Fig. 3, we use the AR-Poisson as a baseline comparison for our ABC model. Given the series of counts from the last 28 days of training data, we forecast ahead $F = 31$ days. We draw $S = 1000$ forecast samples and depict the 2.5^{th}, 50^{th}, and 97.5^{th} percentiles of those samples. We can see that our ABC model has clear advantages over the AR-Poisson, which is limited to capturing linear trends and makes the assumption that the future is like the past.

Appendix F. Details of IHME Baseline forecasts for U.S. States

As a baseline, we consider the public forecasts produced by the IHME COVID-19 forecasting project (Reiner et al., 2021). These forecasts are available online[12] and contain predicted daily occupancy count values for each U.S. state for several stages of hospital care: total beds, ICU beds, ventilators, and deaths.

The core IHME model is targeted at forecasting *deaths* for each U. S. state, using an SEIR compartment model that accounts for a number of local factors. Historical daily death counts represent the primary training data used, though other observed information such as testing and mobility are included. Unlike our approach, the IHME model is not adapted to fit to the observed bed occupancy counts in hospitals in the region of interest. The methodology behind IHME's forecasts for hospital resource use (total bed usage, ventilator usage, etc.) is described in Section 8 of the Supplementary Information (IHME COVID-19 Forecasting Team, 2020) released alongside their published research article on overall forecasting in the United States (Reiner et al., 2021).

To forecast hospital resource utilization, the IHME team performs a "microsimulation" that starts at deaths and works backwards. For each death, they assume the patient stayed the previous 6 days in the ICU. They further simulate for each death, a predicted age bin using local age distribution data, and simulate a number of individuals in the same age group as having also entering the hospital on the same day but surviving. Most of this

12. https://www.healthdata.org/covid/data-downloads

"age-hospital-cohort" stay in the general ward (outside the ICU) for 8 days total. A small fraction of this "age-hospital-cohort" (6.3%) are assumed to be admitted to the ICU and stay for 20 days total (the middle 13 in the ICU). 85% of individuals in the ICU are assumed to need the ventilator. These parametric assumptions are reasonably informed by the literature from a specific location (New York state).

Compared to this approach, we argue that our approach of adapting a flexible hospital model with learnable transition probabilities and durations to a region of interest, rather than simply making fixed assumptions for all states, has substantial benefits.

Comparison of IHME forecasts to our methods. Several factors make it difficult to perform a fair head-to-head comparison between our model and the published IHME forecasts. First, the data signals used to train each method differ: while our method uses counts from all available stages, the IHME model relies primarily on daily deaths. Second, our forecasts require an admission count time series for the test period, while IHME does not. Finally, while our model is open source and can be customized to any training period and any region of interest provided the requisite data, we could not find a way to easily get produce customized forecasts from IHME, so we rely on their published numbers. Thus, any comparison between our methods and IHME should be more of a sanity check than a true comparison of equals. We expect that our method, because it is provided more detailed training data for the region of interest and especially given admissions for the testing period, should outperform the IHME baseline.

Acknowledging these challenges, we try to set up as fair a comparison as possible by taking the IHME forecasts released during our target testing period (Jan. 11 - Feb. 11, 2021), which are the ones dated 2021-01-15 on the IHME website. Manual inspection of the CSV files released on this date indicates that these models had access to death counts until Jan. 11 but not afterwards. We suggest this because before this date values of the "deaths_mean" field in the released spreadsheet are whole numbers, after this date values are fractional indicating an expected value forecast rather than an actual observed count.

Raw forecast information from IHME website. We used the "reference" forecast released by the IHME for 2021-01-15, which provides daily count forecasts of hospital usage for each state of interest. IHME also releases best-case or worst-case projections (imagining different levels of mask usage or movement restrictions), but we did not use these, taking the "reference" forecasts as a reasonable projection of the status quo.

Each field in the released forecast has a "mean", "lower", and "upper" value indicating the expected value as well as lower and upper values to suggest an interval of uncertainty.

We used the following fields of IHME "reference" forecasts.

- admis(mean/lower/upper) : hospital admissions by day
- allbed(mean/lower/upper) : total covid beds needed by day
- ICUbed(mean/lower/upper) : ICU covid beds needed by day
- InvVen(mean/lower/upper) : invasive ventilation needed by day
- deaths(mean/lower/upper) : daily covid deaths

We used the PDF file `IHME_COVID_19_Data_Release_Information_Sheetpdf` included in the ZIP file downloaded from IHME as a "data dictionary" to understand these field names and values.

Standardizing IHME forecasts our data format. We transformed the raw data daily counts to obtain values for our stages by performing the following element-wise subtractions/additions of the above raw data fields:

- General Ward $\mathbf{G}$: allbed - ICUbed
- In ICU without ventilator $\mathbf{I}$: ICUbed - InvVen
- In ICU on ventilator $\mathbf{V}$: InvVen
- In ICU total $\mathbf{I} + \mathbf{V}$: ICUbed
- Terminal $\mathbf{T}$: deaths

MAE computation. To obtain an MAE estimate from IHME at a specific stage $(\mathbf{G}, \mathbf{I}, \mathbf{V}, \mathbf{T})$ for a given state, we look in the testing period simply evaluate the MAE for the mean forecast of that stage compared to our ground-truth count values of that stage (as described in App. A).

Intervals To obtain some estimates of uncertainty, we compute the MAE between the true counts and the lower and upper estimates. This is all we can do given only mean/lower/upper values at each day (rather than a proper distribution).

We emphasize the IHME reported interval is not comparable to the intervals produced by our models. Our model's intervals are more easily interpreted in the standard way: they provide a range of plausible values for what the MAE would be given another similar-sized sample from the posterior.